Relicts of Neo-Tethyan mantle wedge in the Indo-Burma Range, India: Record of carbonate metasomatism and Neo-Tethyan mantle evolution

Oinam Kingson[a,b,c,*], Yongsheng Liu[a], Rajneesh Bhutani[c], Mike Widdowson[d]

[a] State Key Laboratory of Geological Processes and Mineral Resources, School of Earth Sciences, China University of Geosciences, Wuhan 430074, China
[b] Department of Geology, Institute of Sciences, Banaras Hindu University, Uttar Pradesh 221005, India
[c] Department of Earth Sciences, Pondicherry University, Puducherry 605014, India
[d] School of Environmental Sciences, University of Hull, Hull HU6 7RX, UK

ARTICLE INFO

ABSTRACT

Several different geochemical signatures, i.e., mid-oceanic ridge (MOR) and supra subduction zone (SSZ), are frequently reported from ophiolite belts. Such bi-modal geochemical signatures are generally interpreted in terms of formation in two contrasting tectonic settings: divergent and convergent settings with associated petrogenetic processes. Whilst MOR-like and SSZ-like geochemical signatures are well understood in general terms, their combined occurrence in the peridotite component of ophiolite belts is not fully understood. Here, we describe the geochemically comparable Nagaland and Manipur ophiolites which are part of a same belt located in the Indo-Burma Range, India, and represent part of the eastern Tethys regime. In this study we explore the mechanisms which are responsible for this dual geochemical signature in a contiguous ophiolite belt formed during the closure of eastern Neo-Tethys. The existing and new whole-rock Nd isotopic signatures in the serpentinized peridotites from the Manipur ophiolite reveal that the dual geochemical signatures observed in the peridotites are due to patchy metasomatism of the mantle wedge. Thus, the entire mantle section peridotite in the Nagaland and Manipur ophiolites represents a relic of that Neo-Tethyan mantle wedge and this is also supported by the occurrence of high Cs/Th and low U/Th in the serpentinised peridotites. Further, variation of La_N/Yb_N, Sm_N/Hf_N, Ti/Eu, Zr/Hf, Ca/Al and Mg# observed in the secondary and primary clinopyroxenes of the studied peridotites can be explained by an influx of carbonate-rich fluid derived from subducted pelagic limestone. Elemental zoning and associated modeling of clinopyroxenes also clarify that the mantle metasomatism and different degrees of partial melting in the mantle wedge were responsible for the heterogeneity of the Neo-Tethyan mantle preserved in the Nagaland and Manipur ophiolites of the Indo-Burma Range.

1. Introduction

Ophiolites present an accessible, on-shore record through which oceanic crust, and associated oceanic magmatism, crust-mantle interaction, mantle metasomatism, mantle evolution, and wider ancient plate tectonic histories may be investigated (Gass, 1968; Moore and Vine, 1971). Ophiolitic rocks can originate in a variety of oceanic plate tectonic settings ranging from mid-oceanic ridge (MOR) to supra subduction zone (SSZ) to ocean island basalt (OIB) to continental margin (CM) setting, but are particularly well documented from the tectonics associated from the late Mesozoic and early Cenozoic closure of the western Tethys (Dilek and Furnes, 2014; Miyashiro, 1973; Pearce et al., 1984). These differing tectonic settings may be distinguished by geochemical and isotopic signatures in whole-rock and minerals from the mafic and ultramafic rocks of an ophiolite (Pearce et al., 1984; Pearce,

2008; Dilek and Furnes, 2011, Saccani, 2015; Ellam and Hawkesworth, 1988; Workman and Hart, 2005 and reference therein). Subduction-related ophiolites are dominant over other types (i.e., MOR, OIB and CM) largely because the SSZ oceanic lithosphere is relatively buoyant due to its younger age and can therefore be easily detached and obducted onto the continental margin (Miyashiro, 1973; Pearce et al., 1984; Stern, 2004, 2010 and references therein). However, coexistence of distinct MOR- and SSZ-type geochemical signatures within one linear belt of an ophiolite commonly occurs (e.g., Oman, Turkey, Cyprus, Kalayamyo). The origin of these dual geochemical affinities is still not clearly understood and been called the "ophiolite conundrum" (Metcalf and Shervais, 2008). It has been demonstrated that such duality of magmas in ophiolite belts has its origin in the geochemical evolution of melts during subduction initiation (e.g., Dilek and Furnes, 2009; Marchesi et al., 2016; Pirard et al., 2013; Stern, 2004; Whattam and

---

Stern, 2011). At the initial stage of subduction, MORB-like melt is generated from the asthenospheric mantle melting with a relatively insignificant input from the more usually identified subducting slab-derived components (i.e., sediments, and altered oceanic crust.). Accordingly, this earlier MORB- like magma then gets 'overlain' by more typical arc-like calc-alkaline magma which is generated at a later stage with an increasing input of slab-derived fluids/melts (Ishizuka et al., 2014; Reagan et al., 2010).

In contrast with available extrusive and hypabyssal rocks, the origin of the dual geochemical signatures commonly found in the mantle section peridotite is somewhat under investigated, and remains relatively uncertain. Accordingly, the sequence of melt extraction during subduction initiation is poorly understood, and it is challenging to decipher it in ophiolitic mantle peridotite. This is because mantle peridotites generally experience multiple melt extraction episodes, melt/fluid-rock interactions and tectonic fragmentation prior to, and during, emplacement and preservation (Uysal et al., 2016; Wu et al., 2018). However, based on middle REE (MREE) and heavy REE (HREE) abundances in peridotites and clinopyroxenes from the Loma Caribe ophiolite (Dominican Republic), a subduction initiation origin has been inferred. Thus, samples with low MREE/HREE and relatively high MREE/HREE likely record a progressive sequence of melt extractions during subduction initiation (Marchesi et al., 2016). Further interpretation suggested that samples with low MREE/HREE may represent residue after extraction of MORB-like melts from the uplifted asthenospheric mantle with residual garnet, whereas that of the relatively high MREE/HREE are likely residual after extraction of arc-like melts from spinel peridotite. Further, Zhang et al., (2020) claimed that coexistence of high-Cr and high-Al chromite in chromitite is evidence for subduction initiation since genesis of high Al-chromitite and high Cr-chromitite is theoretically linked to the interaction between harzburgite and melts with MORB-like to bonititic compositions (Arai, 1997; Zhou et al., 1996, 1998; Ahmed and Arai, 2002; Ahmed and Habtoor, 2015; Uysal et al., 2009, 2015, 2018).

Such duality of geochemical signatures are similarly observed in the crustal and mantle rocks of the Nagaland and Manipur Ophiolites in the Indo-Burma range, India (Dey et al., 2018; Singh, 2013; Ovung et al., 2018, 2020; Singh et al., 2016). Though, the significant fractionation of MREE/HREE, as observed in the Loma Caribe ophiolite (Marchesi et al., 2016), is not seen either in residual peridotites or its clinopyroxenes (Kingson et al., 2017; Singh et al., 2016, 2013; Dey et al., 2018; Ovung et al., 2020; Abdullah et al., 2018; Ghosh et al., 2018; Ao et al., 2020). In addition, chromite in chromitites of the Nagaland and Manipur ophiolite have high Cr# but no high-Al (Maibam et al., 2017; Pal et al., 2014; Ghosh et al., 2014), which would appear inconsistent with a subduction initiation origin (Zhang et al., 2020). Most recently, Ao et al., (2020) proposed that the serpentinised peridotites in the Nagaland and Manipur ophiolites initially originated in a mid-oceanic ridge setting, and then were modified by slab-derived fluids/melts during subduction processes. Thus, there is scope for an alternative explanation for the origin of the duality of geochemical signatures recorded in the mantle section of the Nagaland and Manipur ophiolite in addition to the existing hypotheses.

Current interpretation of the Nagaland and Manipur ophiolites favours a subduction-related origin (Abdullah et al., 2018; Ao et al., 2020; Kingson et al., 2019, 2017; Maibam et al., 2017; Ovung et al., 2018; Pal et al., 2014). Yet, peridotites in these ophiolites have geochemically diverse signatures (Ghosh et al., 2018); this discrepancy has hitherto been attributed to "mantle heterogeneity" (Batanova et al., 1998; Khedr et al., 2014; O'Driscoll et al., 2018, 2012). Recycling of continental and oceanic components into the mantle during subduction is one of the pivotal mechanisms for generating mantle heterogeneity (Stracke, 2012). Furthermore, mantle metasomatism by fluid/melt derived from the subducting slab at convergent plate margin is commonly considered to be a key mechanism capable of changing the geochemical and mineralogical characteristics of the mantle (Coltorti et al., 2007;

O'Reilly and Griffin, 2013; Roden and Murthy, 1985; Zheng and Hermann, 2014).

Metasomatic reaction between such fluid/melt and the mantle wedge peridotite, with mass transfer taking place at the slab-mantle interface, provides a means of understanding crust–mantle interaction (Li et al., 2013, 2017, 2018; Zheng, 2012). Accordingly, clinopyroxenes in mantle wedge peridotite can thus be utilized to trace the nature of mantle metasomatism because clinopyroxenes are major carriers of incompatible trace elements (Rivalenti et al., 1996). However, with the exception of the work of Ao et al., (2020), geochemical data on clinopyroxene from the Nagaland and Manipur ophiolites are limited. Ao et al., (2020) suggested that melt derived from the subducting basaltic slab metasomatized the overlying mantle which is preserved in the Nagaland ophiolite. However, the geothermal regime during Cretaceous is generally believed to preclude melting of subducting basaltic slab (Peacock, 2013, 1991).

In this work, we focus on two objectives: 1) to better understand the geological processes/mechanisms that cause the observed duality of geochemical signatures of the Nagaland and Manipur ophiolite belt by using published whole-rock geochemical and Nd isotopic data and 2) to document the nature of the Neo-Tethyan mantle metasomatism and its subsequent evolution. For the second objective, in-situ major and trace element concentrations were determined in clinopyroxenes of the serpentinised peridotites from the Manipur ophiolite. We also utilized the existing in-situ major and trace elements data for clinopyroxenes of the peridotites from the Nagaland and Manipur ophiolites.

2. Geological setting

The Nagaland ophiolite and the Manipur ophiolite exposed within the Indo-Burma Range represent part of a suture between the Indian Plate and the Eurasian plate (Fig. 1a and b; Acharyya et al., 1986; Acharyya, 2007, 2010). The Nagaland and Manipur ophiolite belts lie along the southern continuation of the Indus-Yarlung Tsangpo suture zone (IYTSZ) (Fig. 1a), which extends further southward culminating in the currently active Andaman-Nicobar Island subduction system (Fig. 1a; Acharyya, 2015, 2007; Baxter et al., 2011; Fareeduddin, 2015; Ghosh et al., 2017, 2009; Sengupta et al., 1990, 1989; Sloan et al., 2017). The remnants of the Mesozoic Tethyan Ocean that lay between Indian and Eurasia plate are delineated along this older, inactive suture. Accordingly, there are two ophiolite belts to the east of the Indian plate: 1) the ophiolites outcropping along the Myanmar side of the Indo-Burma range representing the eastern belt (Liu et al., 2016a), whereas 2) the ophiolites exposed in the Nagaland and Manipur hills (i.e., the Nagaland and Manipur ophiolite; Singh et al., 2013, 2016, Kingson et al., 2017, 2019) of the Indo-Burma Range, in the Chin Hills of Myanmar (i.e., Kalaymyo ophiolite; Liu et al., 2016a, 2016b), in the Andaman Islands and in the Indonesian outer arc representing the western belt (i.e., Andaman ophiolites; Bhattacharjee, 1991; Curray, 2005; Fareeduddin, 2015; Liu et al., 2016a, 2016b). Recent U-Pb zircon dating suggests that the eastern ophiolite belt represents an older suture of Middle Jurassic age (c 0.173 Ma), which makes it coeval with the Bangong-Nujiang suture in Tibet; in contrast the western belt, that includes the Nagaland, Manipur and Kalaymyo ophiolites, represents the younger IYTSZ of later, Early Cretaceous age (116.4–127 Ma; Aitchison et al., 2019; Liu et al., 2016a; Singh et al., 2017). Throughout the 200 km long and 15–20 km wide Nagaland and Manipur ophiolite belt (Fig. 1b), the exposed rocks appear geochemically consistent (Brunschweiler, 1966).

2.1. Nagaland ophiolite

The NE-SW trending Nagaland and Manipur ophiolite complexes are juxtaposed between two lithologies. These are: 1) Early Ordovician meta-sedimentary rocks of the Nimi Formation to the east (Fig. 2a); and 2) much younger Eocene flysch-like sediments of the Disang Formation
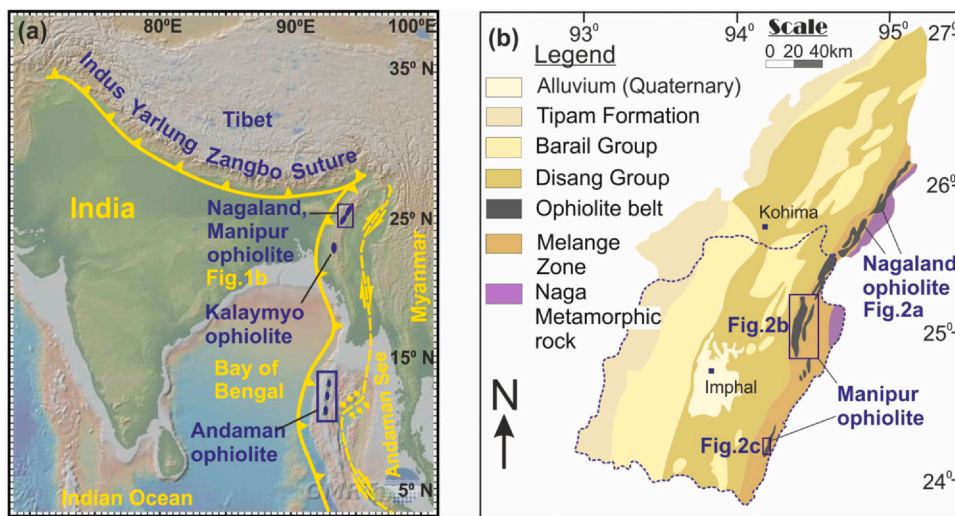
Fig. 1. (a) Regional geological map showing ophiolite distribution along the eastern margin of the Indian plate. This colour shaded map depicting continental and oceanic landform was modified after (Ryan et al., 2009). (b) Geological map of the Indo-Burma Range ophiolites and its associated sediment in Nagaland and Manipur, India (after G.S.I. M.N.C. DRG No. 42/87).

to the west (Fig. 2a). The Nimi Formation comprises meta-sedimentary rocks of blueschist facies metamorphic grade which are an exhumed component of the Burmese continental succession (Ao and Bhowmik, 2014; Fareeduddin, 2015; Ghosh et al., 2014; Kingson et al., 2017). To the west, the Nagaland ophiolite is overlain by the Mid-Late Eocene age Phokphur Formation (Acharyya et al., 1986; Jana and Acharyya, 1986), which is, in turn, overlain by the Eocene Disang Group. The lower, Phokphur Formation consists of ophiolite-derived sediments, sandstone, shale, conglomerate, and coarse sandstone along with minor limestone and carbonaceous material (Ghose et al., 2010). The Disang Group dominantly consists of fine-grained shale intercalated with sandstones and is overlain by the (~1750 m thick) Oligo-Miocene Barail Group (Ghose et al., 2010; Imchen et al., 2014) which is dominantly sandstone with interbedded shale (Vadlamani et al., 2015). The Disang-Barail Groups of rocks are interpreted as flysch-like ocean trench sediments and dominate the Indo Myanmar range (Soibam et al., 2015).

The ophiolite itself is, for the most part, composed of ultramafic rocks (lherzolite, harzburgite dunite, wehrlite and olivine-clinopyroxenite), with sparser exposures of higher-level ophiolite-succession rocks (i.e., pillow basalt, massive basalt, and gabbro), together with minor amount of 'felsic' rocks (i.e., diorite and plagiogranites; Abdullah et al., 2018; Ghose et al., 2014; Pal et al., 2014; Sengupta et al., 1989; Singh et al., 2017). Oceanic pelagic sediments such as chert, marl and limestone are also present in association with the higher-level (extrusive) volcanic rocks. The lower-level ultramafic rocks in the Nagaland ophiolite are variably serpentinised, whilst an eclogite-blueschist assemblage has been reported from the central part of the Nagaland ophiolite belt (Chatterjee and Ghose, 2010; Ghose et al., 2010). This eclogite-blueschist belt has been proposed as portion of an exhumed component of the subducted slab (Acharyya, 2007; Fareeduddin and Dilek, 2015; Kingson et al., 2017). U-Pb zircon dating of plagiogranites and gabbros, yields an age of 116.63 ± 0.30 Ma to 117.55 ± 0.35 Ma for the Nagaland ophiolite (Aitchison et al., 2019; Singh et al., 2017).

2.2. Manipur ophiolite

The Manipur ophiolite is effectively the southern extension of the Nagaland ophiolite (Fig. 1a and b). The northern and the southern ophiolite sections along with their associated lithologies are presented in Fig. 2b and c respectively. The Manipur ophiolite complex presents a typical ophiolite mélange comprising serpentinised peridotites, pelagic sediments, podiform chromitites, mafic rocks and felsic rocks, and is sandwiched between the Late-Cretaceous to Late-Eocene flysch sediments of the Disang Group and molasse sediments of the Barail Group. This ophiolite mélange is overlain by the Disang Group

(Bhattacharjee, 1991). Here, the Disang Group is characterised by the presence of dark grey and black splintery shales which, up-section, become commonly intercalated with siltstone and sandstone (Bhattacharjee, 1991). These flysch-like Disang sediments are, in turn, overlain by the Barail Group which can be distinguished from the Disang Group by the increasing predominance of bedded sandstones intercalated with finer shales.

Variably serpentinised peridotites of the Manipur ophiolite are the dominant exposed component of this ophiolite belt, with minor components of mafic rocks (basalts, gabbros), felsic rocks (plagiogranites) and podiform chromitites. These peridotites are typically harzburgite with lesser lherzolite and wehrlite components (Kingson et al., 2017; Soibam et al., 2015). Varieties of massive, granular, nodular and disseminated chromite have also been reported (Maibam et al., 2017; Pal et al., 2014). U-Pb dating of zircons in plagiogranite and gabbro indicate a crystallization age of c. 117 Ma (Singh et al., 2017; Aitchison et al., 2019), and thus consistent with that of the Nagaland ophiolite (116.63 ± 0.30 Ma to 117.55 ± 0.35 Ma; Singh et al., 2017).

3. Petrography

Although the mantle peridotite and associated tectonite are variably serpentinised, their protoliths are considered to include lherzolite and harzburgite, wehrlite, dunite and pyroxenite (clinopyroxenite and websterite) (Abdullah et al., 2018, Dey e a., 2018; Ao and Satyanarayanan, 2022; Ao et al., 2020, Kingson et al., 2017, Singh et al., 2016, 2013; Fareeduddin1 and Dilek, 2015). Ao et al. (2020) reported two lherzolites which preserve both primary and re-crystallization textures since they display igneous relicts of megacryst clinopyroxene, orthopyroxene, olivine and spinel together with neoblasts of pargasite, clinopyroxene, and also a clinopyroxene veins located in the cracks and grain boundaries of orthopyroxene and olivine phenocrysts (Singh et al., 2016; Ao et al., 2020 and Ao and Satyanarayanan, 2022; Verencar et al., 2021). Clinopyroxene neoblasts, probably secondary in origin, also occur as interstitial grains within the serpentine minerals (Ao and Satyanarayanan, 2022), further demonstrating a complex metasomatic history of these upper mantle rocks.

Similarly, examination of samples MR14–3, −5, −12 and UK14–18 from the current study reveal relict clinopyroxenes (Fig. 3a-h), whilst other phases present include orthopyroxene phenocrysts (Fig. 3 g, h), spinel (Fig. 3e), olivine (Fig. 3d) and serpentinite minerals (Fig. 3a-e and Fig. 3 g, h). Details of these associated minerals are provided in Table 1 and Fig. 3. Clinopyroxene with embayed boundaries commonly occur along the grain boundaries of olivine (Fig. 3d) and orthopyroxenes (Fig. 3f-h) indicating their secondary origin.
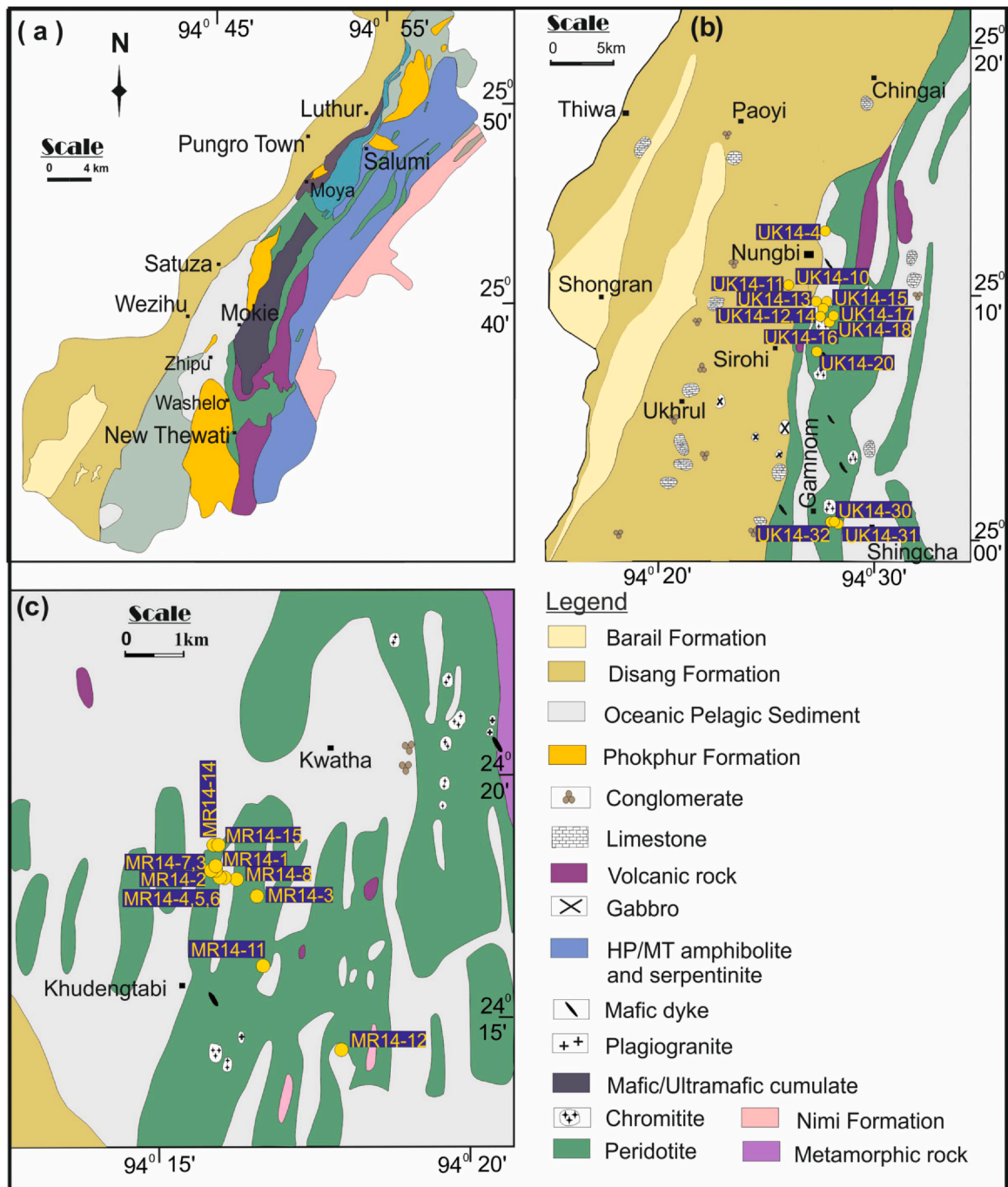
Fig. 2. (a) Geological map of the Nagaland ophiolite modified after Anon., (1986) and (Bhowmik and Ao, 2016). (b) Geological map of the northern part of the Manipur ophiolite, Ukhrul, and (c) Southern part of the Manipur ophiolite, Moreh. The geological maps of the Manipur ophiolite were modified after Singh et al., (2013) and sample locations are marked.

In summary, association of secondary clinopyroxenes with phenocrysts orthopyroxene and/or olivine is generally considered to be the result of interaction of a carbonate-rich fluid/melt with primary olivine and/or orthopyroxene (Coltorti et al., 1999; Ionov et al., 1993; Sun et al., 2012). This type of metasomatic process can typically occur in the mantle wedge during subduction and causes conversion of primary harzburgite or lherzolite to pyroxenite (Liu et al. 2016b) or wehrlite (Coltorti et al. 1999; Green and Wallace, 1988; Yaxley et al., 1991). Therefore, we consider that the clinopyroxenite and websterite present in these Indo-Burma ophiolite belts (Dey et al., 2018; Abdullah et al., 2018, Singh et al., 2016; Fareeduddin, 2015) are likely to have been generated through carbonate-mantle peridotite reaction in slab mantle interface.

4. Methods

Existing major and trace element data for clinopyroxenes in peridotites from the Nagaland and Manipur ophiolites were compiled from Singh et al. (2013, 2016), Abdullah et al. (2018), Ao et al. (2020), Ghosh et al. (2018). In addition, a total of twenty-two serpentinized peridotite samples were also petrographically investigated during this study; four samples (Table 1) (i.e., MR 14–3, −5, −12 and UK14–8) were identified as having fresh clinopyroxenes and selected for further analytical study, and in-situ major and trace elements concentrations were analysed from clinopyroxenes in these samples. New $^{143}Nd/^{144}Nd$ for five serpentinised peridotite samples (i.e., MR14–7, −9 and
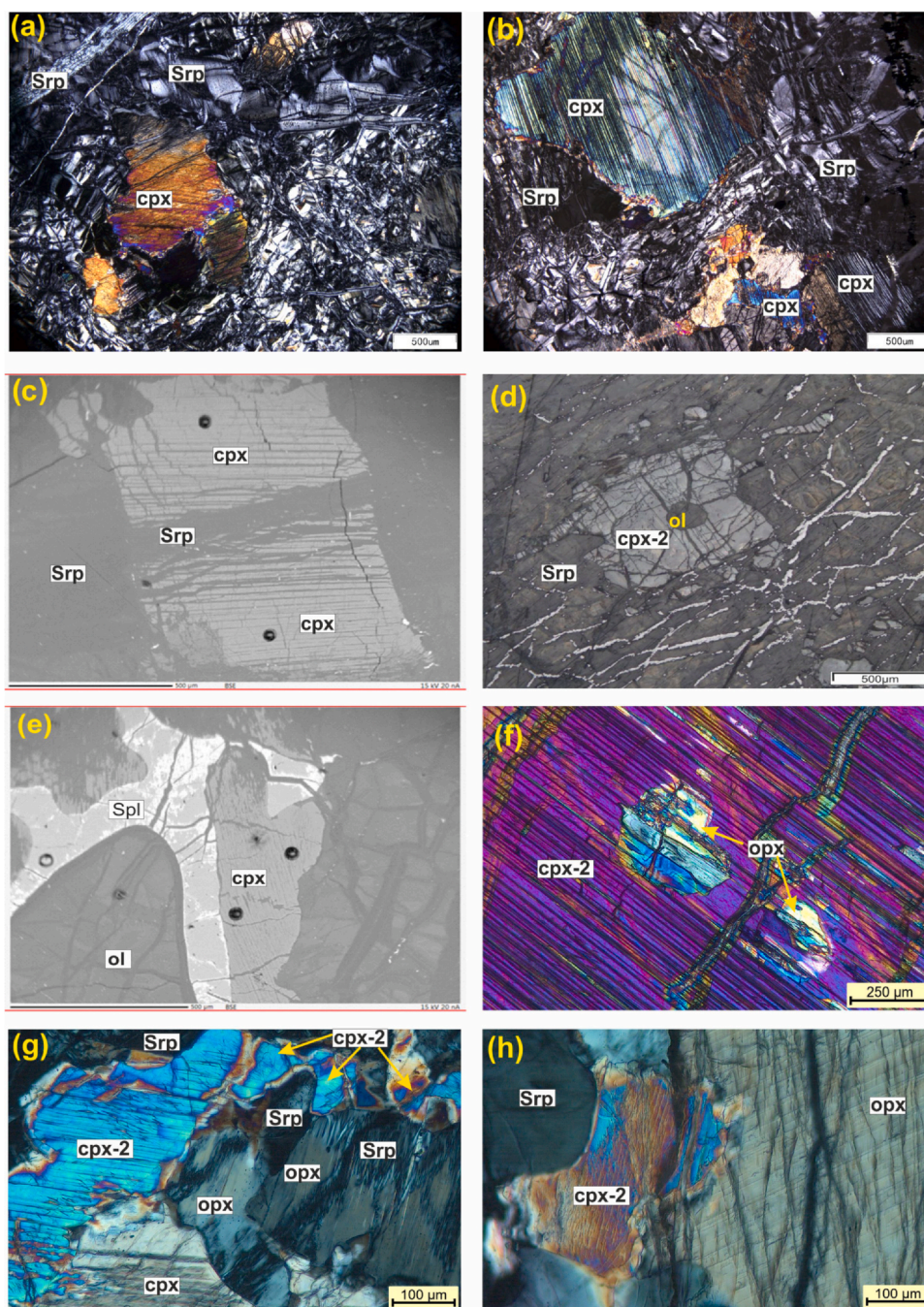
Fig. 3. (a-b) Photomicrographs showing relic clinopyroxenes and serpentine mineral phases in serpentinized peridotites. (c, e and f) BSE images for the relict clinopyroxenes. The spot in the images are the spots where in-situ measurements have been carried out for major and trace elements concentration by LA-ICP-MS. (d) Photomicrograph in reflected light showing relict of olivine surrounded by secondary clinopyroxenes. The abbreviations used in the images; cpx, opx, ol and spt represent clinopyroxene, orthopyroxene and serpentine, respectively. cpx and cpx-2 represent primary and secondary clinopyroxenes respectively.

Table 1
Location and mineralogy of the studied mantle peridotite from the Nagaland and Manipur Ophiolites.

Sample	Location	Lat-Long	Rock	Mineral association	References
Data from literature					
44 A	Nagaland	E94°45.297'; N25°41.747'	Lherzolite	opx, cpx, ol, hbl, spl, srp	Ao et al., (2020)
117 A	Nagaland	E94°45.004'; N25°41.163'	Lherzolite	opx, cpx, ol, hbl, spl, srp	
Data from present study					
MR14–3	Manipur	N24°18′1.54″ E94°15′54.53″	Serpentinised peridotite	opx, cpx, ant, srp, cr-spl, oliv, magt	This study
MR14–5	Manipur	N24°17′52.93″ E94°15′58.47″	Serpentinised peridotite	opx, cpx, srp, cr-spl, oliv, magt	
MR14–12	Manipur	N24°14′19.76″ E94°17′55.88″	Serpentinised peridotite	opx, cpx, srp, Cr-spl, oliv, magt	
UK14–18	Manipur	N25°8′51.96″ E94°27′56.67″	Serpentinised peridotite	opx, srp, cpx, cr-spl	

Note: Abbreviations: opx: orthopyroxene; cpx: clinopyroxene; spl: spinel; ol: olivine; hbl: hornblende; srp: serpentine; cr-spl: chromium spinel; magt: magnetite.

UK14–14, − 17, − 32) were also analysed (Table 1). The neodymium isotope data for other serpentinised peridotite samples used in this study were compiled from Kingson et al., (2017).

4.1. In-situ major and trace element analyses in LA-ICP-MS

In-situ major and trace element concentrations in clinopyroxenes were measured by laser ablation inductively coupled plasma mass spectrometry (LA-ICP-MS) (GeoLas 2005 + Agilent 7700x) at the State Key Laboratory of Geological Processes and Mineral Resources, China University of Geosciences (GPMR-CUG), Wuhan, China. A laser beam of 44 µm was used. Helium was used as a carrier, and nitrogen gas was introduced into the gas flow (Ar + He) of the argon plasma to enhance sensitivity (Hu et al., 2008). The operating conditions for the laser ablation system and Inductively Couple Plasma Mass Spectrometry can be found in Liu et al., (2008). USGS reference materials (BCR-2G, BHVO-2G and BIR-1G) were used for elemental concentration calibration, and a summed metal oxide normalisation was also performed (Liu et al., 2008). Quantitative calibration, off-line selection, integration of the background and analyte signals, and drift correction were conducted using ICPMSDataCal (Liu et al., 2008).

4.2. In-situ major elements analyses in EPMA

In-situ major element concentrations were measured in selected clinopyroxenes and orthopyroxenes of two serpentinized peridotites (i.e., MR 14–5, and − 12) using a CAMECA SX Five electron microprobe analyser (EPMA) at DST-SERB National Facility, Department of Geology, Institute of Science, Banaras Hindu University. A voltage of 15 kV, 10 nA current, and a beam diameter of 1 µm with a LaB6 filament source was applied. A wavelength dispersive spectrometry, along with TAP, LiF, and LPET crystals were used for quantitative analyses. International standards provided by CAMECA-AMETEK were analyzed along with the samples for routine instrument calibration and the detailed procedures and calibration statistics are provided in Pandey et al., (2018). Error on major elements concentrations measurement was < 1%.

4.3. Two pyroxene geothermometry

We applied coexisting clinopyroxene-orthopyroxene geothermometry following the calibration of Taylor (1998) to estimate the temperature of formation of the relict Manipur ophiolite clinopyroxenes. The Taylor (1998) geothermometric equation is a recalibration from that derived by Brey and Köhler, (1990), but using a larger data set and improved activity model which has incorporated the correction for minor components (i.e., Ti, Fe, and Na). It is generally believed that this thermometry provides a reliable mantle temperature estimate because it is more sensitive and precise.

4.4. Whole-rock Nd isotope analysis

Abundances of trace elements are very low in the serpentinized peridotites of the Manipur ophiolite due to their ultra-high depleted nature. Accordingly, 5 – 8 g of powdered sample was digested for Nd isotopic study, but this type of sample volume cannot be readily processed by the normal column procedure for pre-concentration, particularly of Nd and Sm. We therefore applied the method of co-precipitation of lanthanides with iron (Sharma and Wasserburg., 1996), with little modification in the clean isotope laboratory in the Department of Earth Sciences, Pondicherry University, Puducherry, India. The digested dry samples were then re-dissolved with HCl and diluted with Milli-Q first to an ionic strength of ∼1.0. The NH₃ (aq.) was gradually added to the sample solution until a pH value of ∼8 was attained. This solution was thoroughly mixed and kept overnight to allow the precipitates to settle. Then, the supernatant liquid was removed by filtering

the solution through filter papers and the precipitate was re-dissolved with 6 N HCl. The solution contained Fe and REEs, and then Fe was removed by passing the solution through a column filled with the anion exchange resin. For this, the re-dissolved solution was loaded on the pre-calibrated anion exchange resin column equilibrated with 10 ml of 6 N HCl. REEs were collected with 10 ml of 6 N HCl. Nd was separated from the LREEs (light REEs), which were first separated from the total REEs. For separation of LREEs, the dried fraction of the REEs was dissolved in 2 ml of 2 N HCl and loaded on equilibrated Bio-Rad AG50W X8, 200–400 mesh, cation exchange resin column with 15 ml of 2 N HCl. LREEs were collected with 7 ml of 6 N HCl after elution of 40 ml of 2 N HCl and 7 ml of 6 N HCl, as per column calibration. This collected fraction of LREEs was dried and re-dissolved in 300 µl of 0.18 N HCl and loaded on the equilibrated HDEHP-coated Teflon resin column with 20 ml of 0.18 N HCl. Nd was collected with 4 ml of 0.24 N HCl and 6 ml of 0.3 N HCl whereas the Sm was collected in the 0.4 N HCl, after elution of 10 ml of 0.18 N HCl and 6 ml of 0.24 N HCl, as per column calibration. The collected Nd was dried with orthophosphoric acid.

The concentrated dry Nd was loaded on degassed Rhenium filaments after dissolving it with 1 µl of 1 N HNO₃. The $^{143}Nd/^{144}Nd$ isotopic ratios in serpentinized peridotite samples (MR14–7, − 9, UK14–14, − 17, and − 32) were measured using a Thermal Ionization Mass Spectrometer (TIMS, Thermo-Finnigan, model-Triton) housed at the Department of Earth Sciences, Pondicherry University, Puducherry, India. The TIMS measured Nd isotopic ratios with a cup configuration in which ^{146}Nd was measured in the centre cup. Instrumental fractionation was corrected during the run for Nd using exponential law ($^{146}Nd/^{144}Nd$ = 0.7219 for Nd). The measured values for Nd isotope, were corrected for Sm interference, if any, with the present-day ratio ($^{144}Sm/^{147}Sm$ = 0.204800). Nd isotope analysis was achieved with a total of 216 measurements with 12 cycles in 18 blocks. Typically, ∼865 pg was the average procedural blank level for Nd during the sample analysis. The isotope standard AMES was measured during the sample analysis for the $^{143}Nd/^{144}Nd$ ratio and the value was 0.511976 ± 0.000003 (1 sd.; n = 20), which is comparable, though distinct, within the external precision, with the reported value of 0.511960 ± 0.000002 (2σ)(Caro et al., 2006).

5. Results

5.1. In-situ major and trace elements composition

5.1.1. Clinopyroxene
Concentrations of major and trace elements are presented in weight percentage (wt%) and parts per millions (ppm), respectively (supplementary file). The in-situ major elements concentrations which were used for thermometry, are provided in Table 2. In the studied peridotites, clinopyroxenes have the following elemental ranges: SiO₂ (wt%) 49.5 – 51.8, MgO (wt%) 14.19 – 19.51, CaO (wt%) 17.95 – 24.02, Al₂O₃ (wt%) 5.17 – 7.01, TiO₂ (wt%) 0.16 – 0.42, Cr (ppm) 4661 – 9085, Zn (ppm) 4.24 – 17.27, and Ni (ppm) 314 – 758. Ca/Al ratio varies narrowly 2.67 – 4.44, whereas Mg# has a wide variation ranging from 84.41 to 92.00. These relic clinopyroxenes yield flat-HREE and depleted-LREE patterns (Fig. 4e). Cs, Rb, Ba and Pb are enriched whereas Zr, Sr and Ti are depleted when the elemental abundances are normalised to N-MORB (Fig. 4 f).

5.1.2. Orthopyroxene
SiO₂ (wt%) in the orthopyroxenes of the serpentinized peridotites ranges from 51.1 to 55.6, while MgO in the orthopyroxenes ranges from 29.5 to 32.6 wt%. Other major oxides have a small compositional range: Fe₂O₃(T) 5.6 – 6.5 wt%, Al₂O₃ 4.8–6.1 wt%, Cr₂O₃ 0.65–0.78, wt%, CaO 1.7–2.8 wt%, and TiO₂ 0.09–0.14 wt%. Mg# in the orthopyroxenes is moderate and ranges from 89.9 to 90.5.

Table 2
In situ major elements data for clinopyroxenes and orthopyroxenes in the serpentinised peridotites, the Manipur ophiolite.

Sample	MR14-12				MR14-5		MR14-12				MR14-5	
Mineral	Clinopyroxene						Orthopyroxene					
Points	3	4	9	10	31 *	40 *	1	1	5	6	35 *	42 *
SiO2	50.8	50.6	50.7	49.7	49.5	49.3	55.6	55.5	54.5	54.8	53.6	51.2
Na2O	1.00	0.97	0.98	0.90	0.21	0.81	0.09	0.09	0.16	0.10	0.004	0.04
MgO	15.6	15.8	15.5	18.8	15.5	15.9	29.7	30.0	29.5	30.2	31.9	32.6
Al2O3	6.89	6.97	6.93	7.01	5.91	6.00	5.84	5.81	6.07	6.02	4.75	5.03
TiO2	0.32	0.31	0.33	0.30	0.18	0.29	0.12	0.11	0.14	0.12	0.09	0.11
Cr2O3	0.95	1.01	0.98	0.99	1.33	0.98	0.67	0.65	0.67	0.66	0.78	0.68
CaO	21.64	21.39	21.54	18.69	23.18	22.36	1.83	1.70	2.78	1.76	1.88	2.18
MnO	0.10	0.10	0.10	0.11	0.11	bdl	0.15	0.14	0.14	0.14	0.21	0.13
FeO (T)	2.50	2.65	2.73	3.35	2.48	2.63	5.71	5.63	5.76	5.89	6.12	6.52
Total	99.8	98.8	98.8	98.8	98.4	98.2	99.7	99.7	99.7	99.7	99.4	98.4
Oxygen	6	6	6	6	6	6	6	6	6	6	6	6
Si	1.85	1.84	1.85	1.81	1.84	1.83	1.93	1.92	1.90	1.90	1.87	1.82
Na	0.141	0.137	0.139	0.126	0.004	0.015	0.013	0.012	0.022	0.013	0.000	0.001
Mg	0.85	0.86	0.84	1.02	0.43	0.44	1.53	1.55	1.53	1.57	0.83	0.86
Al	0.30	0.30	0.30	0.30	0.19	0.20	0.24	0.24	0.25	0.25	0.15	0.16
Ti	0.009	0.009	0.009	0.008	0.005	0.008	0.003	0.003	0.004	0.003	0.002	0.003
Ca	0.844	0.835	0.841	0.729	0.461	0.445	0.068	0.063	0.104	0.066	0.035	0.042
Mn	0.003	0.003	0.003	0.003	0.002	−	0.004	0.004	0.004	0.004	0.003	0.002
Fe (II)	0.076	0.081	0.083	0.102	0.038	0.041	0.166	0.163	0.168	0.171	0.089	0.097
Mg#	91.8	91.4	91.0	90.9	91.8	91.5	90.3	90.5	90.1	90.1	90.3	89.9

Note: Nd and Sm concentrations used to calculate epsilon values were taken from Kingson et al., (2017). The error is in 1 sigma and is at the last decimal place.

5.2. Whole-rock Nd isotopic composition

$^{143}Nd/^{144}Nd$ isotope ratios were measured for five whole-rocks serpentinized peridotites from the Moreh and Ukhrul sections, Manipur ophiolite (Table 3). The Table 2 present-day $^{143}Nd/^{144}Nd$ ratios have a wide variation ranging from 0.512405 to 0.513192. Age corrected ε_{Nd} (t = 117 Ma) values for the samples vary from − 6.8 to + 5.6.

5.3. Clinopyroxene thermometry

We have estimated the temperature of the formation of the relic clinopyroxenes in two samples of serpentinised peridotites (MR14–12 and MR14–5) based on two-pyroxene geothermometry. The estimated temperature is 1372 ± 7 °C which is high, and thus comparable with the magmatic clinopyroxenes. We assumed a pressure of 14 kbar to calculate the temperature for the formation of these clinopyroxenes. This pressure is within the range (12–16 kbar) estimated from the spinel lherzolite in the Nagaland ophiolite using a P-T pseudosection model (Ao et al. 2020).

6. Discussion

6.1. Metamorphism and its effects on clinopyroxene chemistry

High-pressure metamorphic rocks have been reported from the Nagaland ophiolite; for instance, blueschist, lawsonite-blueschist (Ao & Bhowmik, 2014; Ghose, Agrawal, & Chatterjee, 2010), hornblende eclogite (Bhowmik & Ao, 2016), and eclogite (Chatterjee & Ghose, 2010; Rajkakati et al., 2019; Vidyadharan et al., 1986). It has been suggested that these rocks represent the exhumed part of a subducting slab of oceanic crust in an intra-oceanic subduction system (Bhowmik et al., 2022). The presence of serpentine (Abdullah et al., 2018, Dey et al., 2018; Ao and Satyanarayanan, 2022; Ao et al., 2020, Kingson et al., 2017, Singh et al., 2016, 2013; Fareeduddin1 and Dilek, 2015) and amphibole (Ao and Satyanarayanan, 2022; Ao et al., 2020) in the associated mantle peridotite suggest that these rocks probably experienced greenschist to amphibolite facies metamorphism either in the mantle wedge, or during obduction. In the studied mantle peridotite samples, most of the silicate mineral phases are altered to serpentine minerals but few relict clinopyroxene and orthopyroxene remain preserved (Fig. 3 and Ao et al., 2020). The high LREE and low HFSE in the

secondary, and altered rims around of the primary clinopyroxene (Fig. 4ab; Ao et al., 2020) are likely due to low-temperature secondary processes (i.e., subduction-unrelated serpentinization, carbonation and amphibolitization; Guice et al. 2018; Rollinson and Gravestock, 2012).

Before we discuss subduction zone processes in the mantle wedge based on the in-situ major and trace element data for these relict-clinopyroxenes, it is first necessary to evaluate the effects of post-crystallization alteration in these relict clinopyroxenes and establish the nature of the protolith of these relict minerals. The serpentine minerals clearly formed by hydrothermal alteration, and clinopyroxenes that have interacted with hydrothermal fluids and low temperature carbonate fluids generally display negative Ce-anomaly on chondrite normalised REE plots (Fig. 5). Such negative Ce-anomalies are thought to be generated through addition of La and Pr from the hydrothermal/oxidised fluids, rather than a selective mobilization of Ce out of the mineral/rock (Frisby et al., 2016). However, we observe no significant negative Ce-anomaly in the secondary clinopyroxene, or the rim and core of primary relict clinopyroxene (Figs. 4 and 5); instead, its absence suggests that the fractionation of LREE/HREE in the studied clinopyroxenes (Figs. 4 and 5) is more probably due to primary magmatic processes, subsequent metasomatism and percolation of subducting slab-melt/fluid in a mantle wedge. For comparison, magmatic calcite and dolomite in carbonatites similarly show no negative Ce-anomaly (Fig. 5), further implying that these relict clinopyroxenes are unlikely to have been influenced by low-temperature hydration and carbonation processes during emplacement and obduction of these rocks. To further confirm that the relict clinopyroxene retains essentially magmatic characteristics, petrographically unaltered areas were identified and major and trace element concentrations were thoroughly analyzed using back scattered electron (BSE) imaging. No alteration products (i.e., secondary minerals such as chlorite, serpentines and amphibole) were discovered at or near the analyzed spots within the clinopyroxenes (Fig. 3c and e; see also the petrographic section of Ao et al., 2020). Therefore, major post-crystallization changes due to low-temperature hydration processes are unlikely.

In terms of mineral geochemistry, it is known that 'relict' clinopyroxenes present in serpentinised peridotite can be of secondary/non-magmatic formed by the interaction of hydrothermal fluids during the serpentinization processes after emplacement and obduction of the ophiolitic rocks. Such hydrothermal non-magmatic clinopyroxenes are reported in peridotites (Python et al., 2007) and gabbro (Akizawa et al.,

O. Kingson, Y. Liu, R. Bhutani et al.
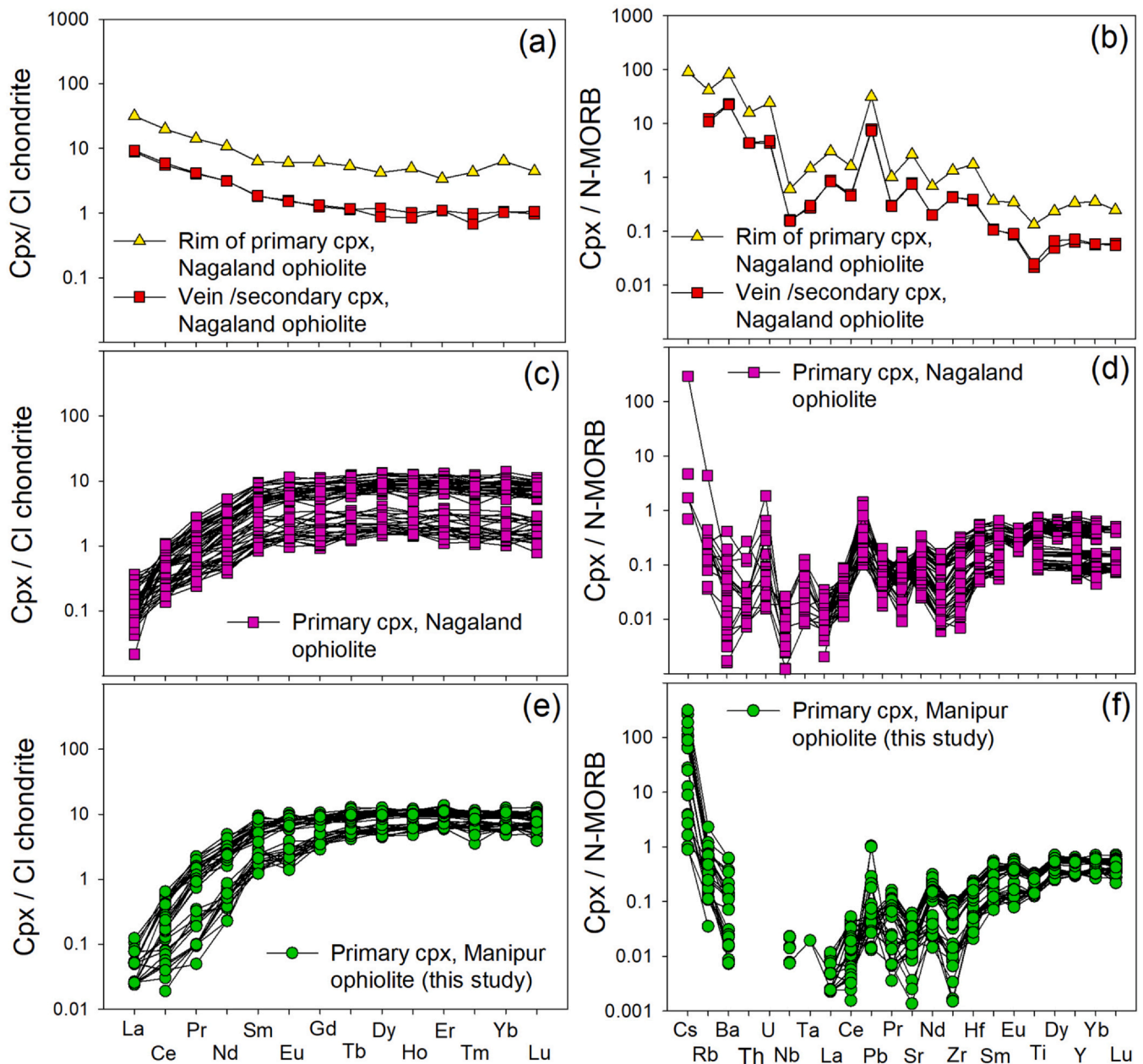
Fig. 4. (a-b) Cl chondrite normalised REE patterns and N-MORB normalised trace elements patterns for secondary/vein clinopyroxenes and rim of the primary clinopyroxenes of the peridotites from the Nagaland. REE and trace element patterns normalised to Cl chondrite and N-MORB for the primary clinopyroxenes of the serpentinised peridotites in the Nagaland ophiolite (c-d) and Manipur ophiolite (e-f). The normalising trace elements data were taken from (Sun and McDonough, 1989). The In-situ major and trace element concentrations for the clinopyroxenes of serpentinised peridotites in the Nagaland ophiolites were compiled from Ao et al. (2020).

2011) of the Oman ophiolite. These non-magmatic clinopyroxenes are characterised by 1) very low Cr_2O_3 (average = 0.05 wt%) & Al_2O_3 (average = 0.3 wt%), and 2) positive Ce and/or Eu anomaly in

Chondrite normalized REE patterns (Python et al., 2007; Akizawa et al., 2011). In contrast with these, the relict clinopyroxenes from this study display high Cr_2O_3 (0.47–0.91 wt%; average = 0.67 wt%) and Al_2O_3

Table 3
Nd isotopic ratios in serpentinised peridotites, Manipur ophiolite, Indo-Burma Range, India.

Sample ID	Nd (ppm)	Sm (ppm)	$^{143}Nd/^{144}Nd$	$f^{Sm/Nd}$	ε_{Nd} (t = 117 Ma)
MR14–7	0.008	0.005	0.512427 ± 5	0.43	-6.8
MR14–9	0.07	0.065	0.513167 ± 2	1.82	4.9
UK14–14	0.022	0.011	0.512760 ± 4	0.34	0.8
UK14–17	0.046	0.044	0.513067 ± 2	1.84	2.7
UK14–32	0.079	0.071	0.513192 ± 3	1.65	5.6

Note: * Represent the in situ major elements data from EPMA analysis. Major elements contents are presented in weight percentage, whereas the rest of the data were obtained from LA-ICP-MS.
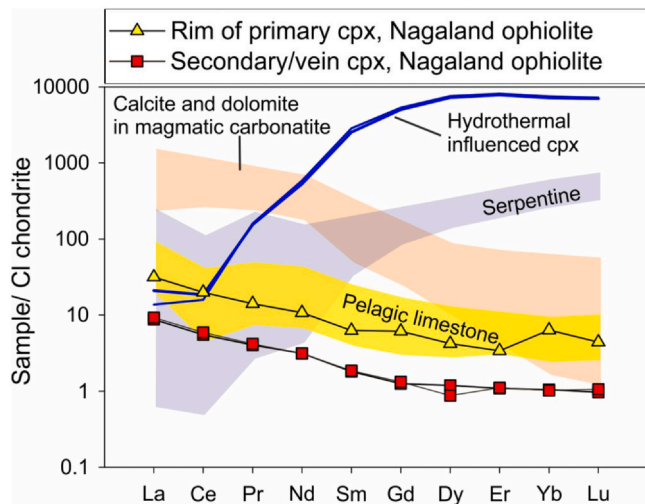
Fig. 5. Cl chondrite normalised REE patterns for the rim of primary cpx and secondary cpx of the peridotites from the Nagaland. We also plotted serpentine and altered clinopyroxene in abyssal peridotite (after Frisby et al., 2016), pelagic limestone from Manipur ophiolite (after Singh et al., 2016) and calcite-dolomite in carbonatite (after Xu et al., 2008) for comparison. The normalising REE data were taken from (Sun and McDonough, 1989).

(5.2–7.1 wt%; average = 6.0 wt%) and, as indicated above, have no Ce and Eu positive anomaly in chondrite normalised-REE patterns (Figs. 4 and 5). These geochemical features in the studied clinopyroxenes agree with the composition of magmatic/mantle peridotitic clinopyroxenes which have Cr_2O_3 (0.5–2.5%), Al_2O_3 (> 1.5%) (Python and Ceuleneer, 2003; Ernewein et al., 1988 and Petrological database of the ocean floor, 2001).

To summarize, we are confident that the clinopyroxenes in this study are magmatic in origin; the high formation temperature for these clinopyroxenes (1372 ± 7 ^{0}C) obtained from the coexisting clinopyroxene-orthopyroxene geothermometry is inconsistent with secondary processes and their composition likely recorded geochemical changes in the mantle wedge. Accordingly, their geochemistry can be further utilized to understand slab-mantle interface-related processes in the subduction setting.

6.2. Dual tectonic settings fail to explain the compositional variations of the serpentinised peridotite

A duality of ophiolite geochemical signatures was first recognized in the Semail ophiolite (Alabaster et al., 1982). The origin of these dual geochemical affinities in a single belt was not initially understood, and became known as the so-called "ophiolite conundrum" (Metcalf and Shervais, 2008). Evidence for the origin of the dual geochemical signatures has subsequently been reported from locations such as the
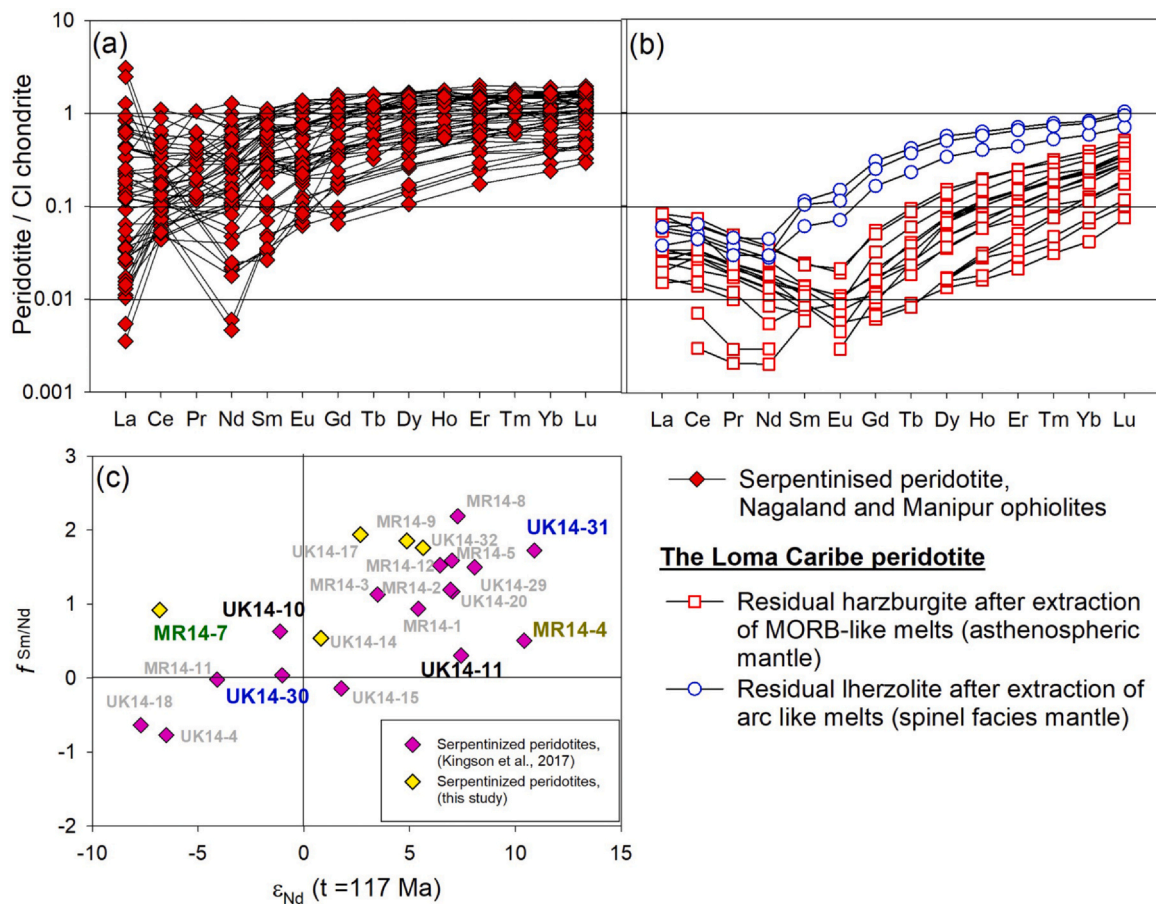
Fig. 6. (a) Cl chondrite normalised REE patterns of all the available data for the serpentinised peridotites in the Nagaland and Manipur ophiolites. The peridotites data were taken from Kingson et al., (2017), Verencar et al., (2021 and 2022), Singh et al., (2013, 2016). (b) REE patterns normalised by Cl chondrite for the inferred harzburgite with residual garnet facies (i.e., uplifted asthenospheric mantle) and spinel facies peridotites from the Loma Caribe ophiolite, Dominican Republic for comparison. The peridotite bulk rock data were taken from Marchesi et al., (2016). The normalising values were taken from (Sun and McDonough, 1989). (c) ε_{Nd} (t = 117) versus $f^{Sm/Nd}$ variation plot for all the available serpentinized peridotite samples from the Manipur ophiolite. Nd and Sm concentrations used for calculation of ε_{Nd} and $f^{Sm/Nd}$ were taken from Kingson et al., (2017). The $^{143}Nd/^{143}Nd$ isotope ratios for all the samples were taken from Kingson et al., (2017), except the $^{143}Nd/^{143}Nd$ isotope ratios MR 14–7, − 9, − 12 and UK14–14, − 17, and − 32 samples.

ARTICLE IN PRESS

O. Kingson, Y. Liu, R. Bhutani et al.   Results in Earth Sciences xxx (xxxx) xxx

modern Izu-bonin Mariana arc system, and the western Tethyan ophiolites of Oman, Greece and Albania (Ishizuka et al., 2011; Reagan et al., 2010; Whattam and Stern, 2011), and Cyprus (Pearce and Robinson, 2010). In these settings, the lava generated at the initial stage of subduction is MOR-like and is known as 'forearc basalt' (Reagan et al., 2010). However, this MOR-like basalt and intrusive equivalents are later overlain by increasingly arc-like extrusive rocks and both are commonly intruded by the latest-stage boninitic-type dykes (Whattam and Stern, 2011). In effect, the magmatism changes from MORB to a nascent 'arc-type', (i.e., boninitic composition). However, whilst such explanations for geochemical duality have been previously reported for oceanic-crustal rocks, the causes of duality of geochemical signatures in mantle peridotites, such as observed in the Nagaland and Manipur ophiolites, remains under investigated (Dey et al., 2018; Singh, 2013; 2016; Ovung et al., 2018, 2020).

Based on the fractionation of MREE/HREE in peridotites and its clinopyroxenes of the Loma Caribe ophiolite, Dominican Republic and variable composition of Cr# in chromitite of the Zambales ophiolite, Philippines, Marchesi et al., (2016) and Zhang et al., (2020) claimed that the dual geochemical signature in the mantle rocks were a consequence of a succession of melt extraction during subduction initiation. However, the significant fractionation of MREE/HREE, observed in the Loma Caribe ophiolite (Fig. 6b), is not observed in both residual peridotites (Fig. 6a) and its clinopyroxenes (Fig. 4) in the Nagaland and Manipur ophiolites. Further, chromite in the chromitites of our examples have high-Cr (i.e., Cr# = 63.6–82.0), but do not show high-Al (Maibam et al., 2017; Pal et al., 2014; Ghosh et al., 2014), so are similarly inconsistent with the subduction initiation origin (Zhang et al., 2020). The underlying principle of the subduction initiation explaining high-Cr# (72.9–75.9; Zhang et al., 2020) and high-Al (Cr# = 45.5–47.7; Zhang et al., 2020) in chromitites is that they could have been formed by the interaction of peridotite with MORB-like and boninite melts, respectively, during subduction initiation (Zhang et al., 2020).

Interestingly, two samples, UK14–30 and UK 14–31, collected from the same outcrop in the Manipur ophiolite (Fig. 1c and Table 4) show contrasting isotopic and geochemical signatures (Fig. 6c). UK14–30 displays a slightly U-shaped REE pattern with low ε_{Nd} (t) (−1.0), whereas UK14–31 shows depleted-LREE pattern with high ε_{Nd} (t) (+10.9) (Fig. 6c). The former is believed to represent a metasomatized mantle source in a subduction setting (e.g., Ellam and Hawkesworth, 1988), whereas the latter is from a typical depleted mantle source generally proposed to have formed in a MOR setting (Workman and Hart, 2005 and references therein). However, the UK14–31 sample was collected from c.335 m away from the other sample (UK14–30) and both outcrops, near Gamnom, Ukhrul, had physical continuity (Fig. 2b and Table 4). Similar geochemical features for other samples are also observed in different sections of the Manipur ophiolite (Fig. 2b and c) and details are provided in Table 4. In addition, when ε_{Nd} (t) values of all the available peridotite samples are plotted against their $f^{Sm/Nd}$ (Fig. 6c), a continuous trend indicating a positive correlation is observed without any compositional gap. Such a continuous trend could have resulted from variable extents of metasomatism in the same

mantle wedge (Kingson et al., 2017). The samples with high and positive ε_{Nd} (t) and low $f^{Sm/Nd}$ could have been unaffected by the subduction components. In contrast, other samples with negative ε_{Nd} (t) and low $f^{Sm/Nd}$ correspond to a portion of the same mantle wedge dominantly influenced by subduction components. Based on these isotopic and geochemical features, the earlier studies in which the peridotite of the Manipur ophiolite were suggested to have been formed in MOR and SSZ settings (Ningthoujam et al., 2012; Ibotombi et al., 2013, Singh et al. 2013, 2016; Ovung et al., 2018) have been re-interpreted to have been derived from a single source (Kingson et al. 2017).

It is generally thought that the fluid/melt derived from a subducting slab does not traverse the entire mantle wedge (Spandler and Pirard, 2013). So it would be reasonable to expect that the entire mantle wedge is not entirely converted to metasomatized materials. More likely there would remain portions of unmetasomatized mantle wedge and that these two closely associated portions (i.e., metasomatized and un-metasomatized) could later be obducted together to form the variety of mantle materials now preserved in the present-day subduction-related ophiolite mélange. Therefore, we propose that the existence of dual geochemical signatures (i.e., MOR and SSZ-like geochemical affinities) observed in the peridotites of the Nagaland and Manipur ophiolites, and previously believed to have originated in two contrasting tectonic settings (i.e., MOR and SSZ; Ningthoujam et al., 2012; Ibotombi et al., 2013, Singh et al. 2013, 2016; Ovung et al., 2017; Dey et al., 2018, Ao et al., 2020), are most likely to have resulted from "patchy metasomatism" in the mantle wedge. This would then account for the geochemical variability in the Nagaland and Manipur ophiolites.

6.3. Origin of clinopyroxene and carbonate metasomatism

All available data for the serpentinised peridotites in the Nagaland and Manipur ophiolites in the U/Th vs. Cs/Th variation plot (Fig. 7; after Peters et al., 2017), are clustered towards the field of forearc serpentinite, thus substantiating its origin in the mantle wedge (Peters et al., 2017). Kingson et al., (2017, 2019) have also shown that the rocks in the Nagaland and Manipur ophiolites were generated from a fluid-metasomatized mantle source in a subduction setting based on elemental and isotopic abundances in the mafic and ultramafic wholerocks; however, the composition of the metasomatic agents derived from the subducting slab which had fluxed the mantle wedge is not been discussed in detail by these authors. More recently, based on trace element contents in clinopyroxenes of peridotites, Ao et al., (2020) proposed that silicate melts derived from the subducting basaltic slab had fluxed the mantle wedge causing both modal (i.e., changing the mineralogy) and cryptic (i.e., without changing the mineralogy) metasomatism in the peridotites of the Nagaland ophiolite. Modal metasomatism in the peridotites of the Nagaland ophiolite is evidenced by the presence of locally developed clinopyroxenes and amphiboles which show LREE-enriched patterns, high Sr/Y, and depletion in Nb and Ti. In contrast, the cryptic metasomatism is evident from the orthopyroxene and clinopyroxene rims (i.e., LREE-enriched, high Sr/Y, and depletion in Nb and Ti) adjacent to the secondary clinopyroxenes (Ao et al., 2020). However, the idea of derived silicate melts affecting

Table 4

Sample location of closely associated peridotites along with their latitude and longitude. Distance between closely associated samples and their ε_{Nd}(t = 117 Ma) are also presented.

Location	Sample ID	Latitute	Longitude	ε_{Nd} (t)	Distance between two samples (m)
Between Sirohi and Nungbi, Ukhrul	UK14–10	N25°10′22.25″	E94°26′2.65″	-1.1	< 2
	UK14–11	N25°10′22.25″	E94°26′2.65″	7.4	
Near Gamnom, Ukhrul	UK14–30	N25°0′40.1148″	E94°28′20.852″	-1.0	~335
	UK14–31	N25°0′45.33″	E94°28′10.33″	10.9	
Imphal to Moreh road (NH 102), near Moreh town	MR14–7	N24°17′52.49″	E94°16′2.97″	-6.8	~127
	MR14–4	N24°17′52.93″	E94°15′58.47″	10.4	

Note: Nd isotopic ratios of UK14-10, UK14-11, UK14-30, UK14-31 and MR14-4 were taken from Kingson et al., (2017).
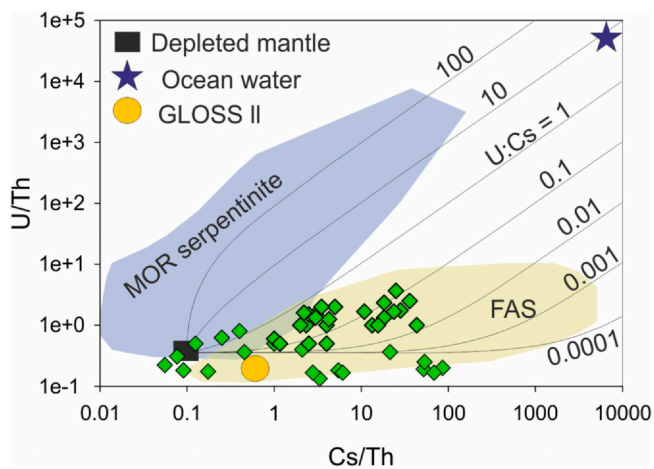
Fig. 7. U/Th vs Cs/Th variation diagram for the studied serpentinised peridotites after Peters et al., (2017). The MOR-serpentinite and forearc serpentinite (FAS) fields were constructed based on the compiled data of Peters et al., (2017). This plot clearly suggests that the serpentinised peridotites in the Nagaland and Manipur ophiolites represent mantle wedge serpentinite rather than MOR-serpentinised peridotite. Primitive mantle (Palme and O'Neill, 2014), Depleted mantle (Salters and Stracke, 2004), GLOSS ll (Plank, 2014) and ocean water (Li, 1991) values are plotted for comparison.

the mantle source of the Nagaland ophiolitic rocks are unlikely for the following reasons: (1) Melting of subducting basaltic slab is at odds with the thermal structure of modern subducted slabs (Peacock, 2013, 1991). (2) Residual clinopyroxenes in peridotites after partial melting (Baker and Stolper, 1994; Falloon et al., 1999; Schwab and Johnston, 2001; Walter, 1998; Wasylenki, 2003; Gaetani and Grove, 1998; Pickering-Witter and Johnston, 2000) should have Ca/Al < 5 and Mg# < 92, similar to the clinopyroxene which interacted with an experimental high silicate melt derived from eclogite (i.e., subducting basaltic slab; Wang et al., 2010; Yaxley et al., 1991). By contrast, the secondary clinopyroxenes reported by Ao et al., (2020) show variable and high Ca/Al (6.6–9.3) and Mg# (95.99–99.68) which are inconsistent with the melt-mantle interaction model. (3) The high Sr/Y and La/Yb can be generated by a variety of petrological processes in magmatic rocks (Moyen, 2009), for instance, melting of the basaltic crust on the subduction slab, which would then give rise to adakite compositions displaying these high ratios.

Alternatively, the inferred metasomatism in the mantle wedge of the Nagaland ophiolite could be caused by adakite melts (i.e., melt having high Sr/Y) derived from the subducting basaltic slab (Ao et al., 2020). Therefore, to test this idea, we re-evaluate the results of the secondary clinopyroxenes and rims of relict primary clinopyroxenes reported in the Nagaland peridotite. On careful scrutiny, the chemistry of these secondary clinopyroxenes and clinopyroxene rims which have high La/Yb (7.0–12.6), Zr/Hf (27.9–42–9), Ca/Al (6.6–9.3), Mg# (96.0–99.7), and low Ti/Eu (1880–2891), are consistent with carbonate-derived metasomatism in the mantle, as shown by Rudnick et al., (1993). Additionally, Klemme et al., (1995) further suggested that Ti/Eu ratios in clinopyroxenes are particularly sensitive to trace carbonate metasomatism. Therefore, the observed geochemical features in our secondary clinopyroxenes indicate that the fluid/melt would likely be carbonate-rich rather than from a silicate melt derived from subducting basaltic slab (Fig. 8a-d; Coltorti et al., 1999; Gervasoni et al., 2017; Klemme et al., 1995; Rudnick et al., 1993; Zong and Liu, 2018). Further, the composition of the secondary clinopyroxenes lies in the field of carbonate-metasomatism on Ti/Eu vs. La/Yb and Ca/Al vs. Mg# plots (Fig. 8a and d), indicating the influx of carbonate-rich fluid/melt into the mantle wedge; high Zr/Hf and its correlated changes with La_N/Yb_N in the secondary clinopyroxenes and rim of relict primary clinopyroxenes also support this inference (Fig. 8b). The inferred carbonate

metasomatism is also supported by observed depletion in Nb and Ta compared to La and depletion in Ti compared to Sm in N-MORB normalised patterns for secondary clinopyroxene and rim of primary clinopyroxene (Fig. 9a). The depletion in Nb, Ta and Ti could also have resulted from the fractionation of amphibole and rutile, respectively (Rivalenti et al., 1996). However, the depletion in Nb and Ta compared to La is observed in both coexisting secondary clinopyroxenes and amphiboles (Fig. 9a and b), which indicates that fractionation of amphibole could not produce the required depletion in Nb and Ta in the studied clinopyroxenes. Rutile is not reported in the Nagaland and Manipur ophiolites and can thus be rejected to explain Ti depletion in the clinopyroxenes.

An influx of slab-derived carbonate-rich fluid/melt into the mantle wedge is also texturally supported. Interaction of carbonate rich fluid/melt with the orthopyroxenes and/ olivine (Dalton and Wood, 1993) always results in the formation of secondary clinopyroxenes (Coltorti et al., 1999; Ionov et al., 1993; Sun et al., 2012), which is evident by the formation of few secondary clinopyroxenes in the cracks and grain boundaries of the orthopyroxenes (Fig. 3f-h and see the Fig. 5 of Ao et al., 2020) and olivine (Fig. 3d). This type of secondary clinopyroxene (i.e., clinopyroxenes having high La/Yb and Zr/Hf) is hitherto unreported in the peridotites of the Manipur ophiolite. However, the major and trace element abundances in clinopyroxenes (i.e., high Ca/Al ratios (> 5) and depletion in Nb, Zr and Ti) (Figs. 4 and 8d) suggests carbonate metasomatism in these mantle peridotites. Some of the clinopyroxenes of the Nagaland and Manipur ophiolitic peridotites also show correlated changes of Sm_N/Hf_N with Zr/Hf such that the data fall in the field for well-known carbonate-metasomatized clinopyroxenes (Chen et al., 2017; Wu et al., 2017; Guo et al., 2020; Deng et al., 2017) of the mantle xenoliths from the China craton (Fig. 8c). These features are further indicative of interaction of carbonate-rich fluid/melt with the mantle wedge peridotites. In addition, the composition of the carbonate-melt equilibrated with clinopyroxenes is similar in their trace elements patterns with secondary clinopyroxenes and rim of the primary clinopyroxene (Fig. 10), substantiating the inferred carbonate metasomatism. The parameters used in this model are described in figure caption (Fig. 10).

Some of the primary clinopyroxenes fall outside the carbonate metasomatized fields (Fig. 8a, c, d), and more clearly follow a melting trend (Fig. 8c). In addition, LREE depletion is observed in these primary clinopyroxenes (Fig. 4), instead of LREE enrichments expected from carbonate metasomatism. Such geochemical features could have been produced by larger degrees of melt extraction from the carbonate metasomatised mantle source - a scenario supported by the melting model (Fig. 13). The residual clinopyroxenes, after variable degrees of partial melting (1%−20%), generated from the carbonate-metasomatized mantle source are comparable with the depletion of LREE observed in the studied clinopyroxenes. Details of the melting model are explained in Section 6.5 and Fig. 13.

6.4. Origin of carbonate-rich fluid/melt

Carbonate-rich fluid/melt derived from upwelling asthenosphere (deep-mantle) is generally characterized by steep LREE-enriched patterns with enriched incompatible trace elements (e.g., Th, Nb, Ta, Sr; Jones et al., 2013). Such geochemical characteristics are dissimilar to trace elements abundances in the secondary clinopyroxene and rim of the primary clinopyroxene (Fig. 4a-b and Fig. 11); therefore, it is unlikely that the carbonate-rich fluid/melt that had interacted with the studied peridotites originated from the upwelling asthenosphere. By contrast, the composition of melts derived from carbonated pelite and eclogite are mainly controlled by felsic minerals and rutile respectively (Meinhold, 2010; Pfänder et al., 2007). Thus, the melts derived from the carbonated pelite and eclogite generally have high Th and Nb, respectively. However, the secondary clinopyroxene and rim of the primary clinopyroxene display depletion in Th and Nb in N-MORB

ARTICLE IN PRESS

O. Kingson, Y. Liu, R. Bhutani et al.   Results in Earth Sciences xxx (xxxx) xxx
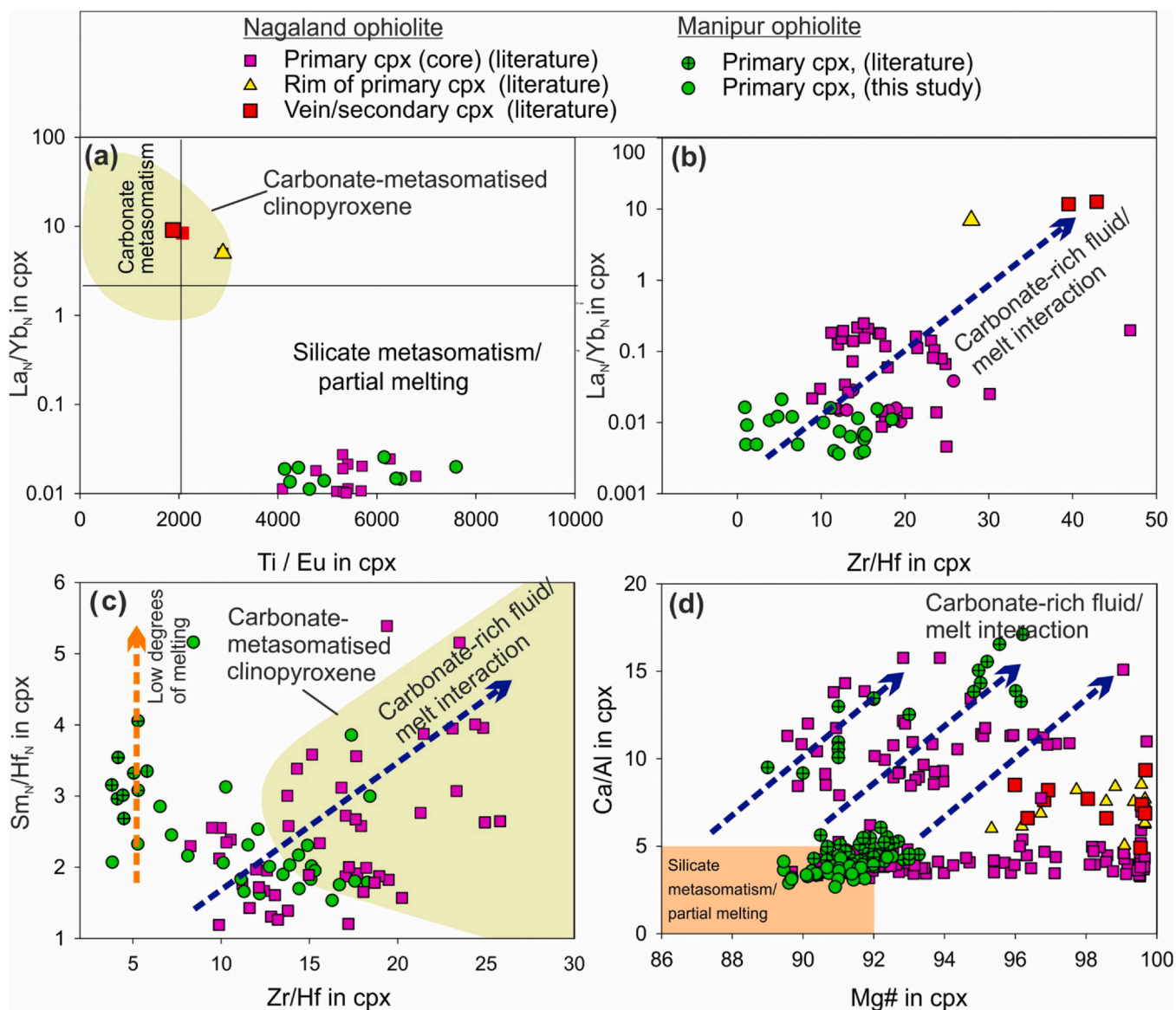
Fig. 8. (a) La$_N$/Yb$_N$ versus Ti/Eu variation plot for clinopyroxenes of peridotites from the Nagaland and Manipur ophiolites. Field for the carbonate-metasomatised clinopyroxene was constructed based on the compiled data of well-known carbonate-metasomatised clinopyroxenes in the mantle xenoliths from the North China Craton (Zhong and Liu, 2018). (b) Variation plots of La$_N$/Yb$_N$ against Zr/Hf in clinopyroxenes of the peridotites from the Nagaland and Manipur Ophiolites. The observed positively correlated changes between La$_N$/Yb$_N$ and Zr/Hf in clinopyroxenes suggest carbonate metasomatism. (c) Sm$_N$/Hf$_N$ versus Zr/Hf variation plot in clinopyroxenes and comparison of the clinopyroxenes in the peridotites of Nagaland and Manipur ophiolites with well-known carbonate-metasomatised clinopyroxenes of the mantle xenolith from China Craton (Chen et al., 2017; Wu et al., 2017; Guo et al., 2020; Deng et al., 2017). (d) Ca/Al versus Mg# diagrams for all the available and new clinopyroxenes data of the peridotites from the Nagaland and Manipur ophiolites. Subscript "N" in the plots represent N-MORB normalisation and the normalising values were taken from Sun and McDonough, (1989). The existing major and trace elements data for clinopyroxenes of the Nagaland and Manipur ophiolites were taken from Singh et al., (2013, 2016); Abdullah et al., (2018); Ghosh et al., (2017); Ao et al., (2020).

normalised spider diagram (Fig. 11). Such geochemical signatures in the clinopyroxene indicate that the carbonate-rich fluid/melt that has metasomatised the mantle wedge in the subduction setting could not have been originated from the carbonated pelite and eclogite.

Alternatively, N-MORB normalized trace element patterns of the secondary clinopyroxene and primary clinopyroxene rim, that is Rb, U, Sr enrichment and HFSE (Th, Nb, Zr, Hf, Ti) depletion, are comparable with that of limestone (Fig. 11). Accepting this, and arguments detailed above, the geochemical signatures are more consistent with the limestone derived carbonate-rich fluid/melt assisted metasomatism of the mantle wedge - barring only a couple of elemental abundances, such as the relative enrichment in Ta and Ba. A possible explanation is that the Ta enrichment relative to Nb observed in the secondary clinopyroxenes (Fig. 11) could be resulted by influence of rutile bearing eclogite-

derived fluid (Huang et al., 2012; Kingson et al., 2019; Munker et al., 2004), though this remains to be confirmed, whilst the observed Ba enrichment (Fig. 11) could have been modified by fluids derived from subducted siliciclastic sediment (Plank and Langmuir, 1998).

To summarise, the generation of carbonate-rich fluid through dissolution of carbonate minerals has generally been considered to play a minor role in slab-mantle interface in subduction setting (Poli et al., 2009). However, high pressure experimental research has demonstrated that subduction zones can provide the conditions necessary to readily dissolve subducted calcite or aragonite in the presence of aqueous fluids (Caciagli and Manning, 2003; Dolejš and Manning, 2010). Frezzotti et al., (2011) subsequently demonstrated that dissolution of subducted-carbonate minerals in slab-derived fluids, even in the carbonate stability condition, is a pivotal mechanism that transfers carbon into the

ARTICLE IN PRESS

O. Kingson, Y. Liu, R. Bhutani et al.   Results in Earth Sciences xxx (xxxx) xxx
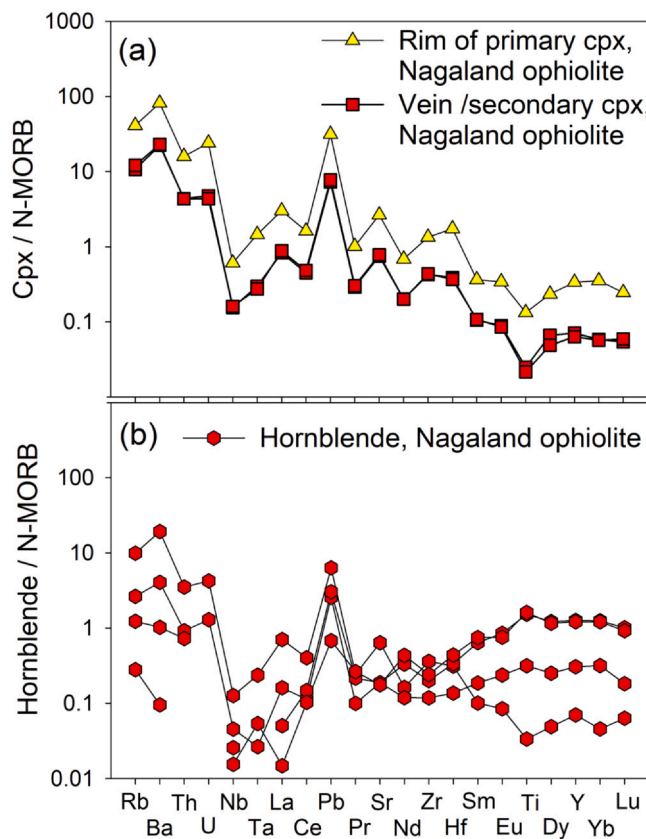
Fig. 9. N-MORB normalised trace elements patterns for secondary clinopyroxenes, rim of primary clinopyroxene and secondary hornblendes (pargasite) in the peridotites from the Nagaland ophiolite. The N-MORB normalising values were used from Sun and McDonough, (1989).
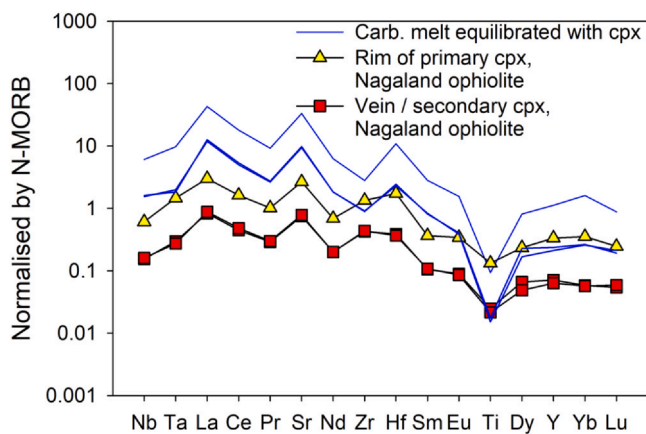
Fig. 10. N-MORB normalised trace elements patterns for secondary clinopyroxenes, rim of primary clinopyroxene and its comparison of the carbonated melt equilibrated with these clinopyroxenes. The N-MORB normalising values were used from Sun and McDonough, (1989). Partition coefficients used for the calculation of carbonate melt equilibrated with clinopyroxenes in the peridotite are from Adam and Green (2001) and Klemme et al. (1995). The trace elements concentrations in these clinopyroxenes were taken from Ao et al., (2020). Abbreviations: Carb.: Carbonate; cpx: clinopyroxene.

overlying mantle in subduction setting. Poli, (2015) suggested that Ca-rich carbonate fluids can be generated at temperature ranging from 870 °C to 900 °C, representing a shallow depth of ~120 km in the mantle below arc in subduction setting. Therefore, we conclude that carbonate-rich fluid, even in carbonate stability condition, can be generated from the subducted limestone and transfer fluid-mobile
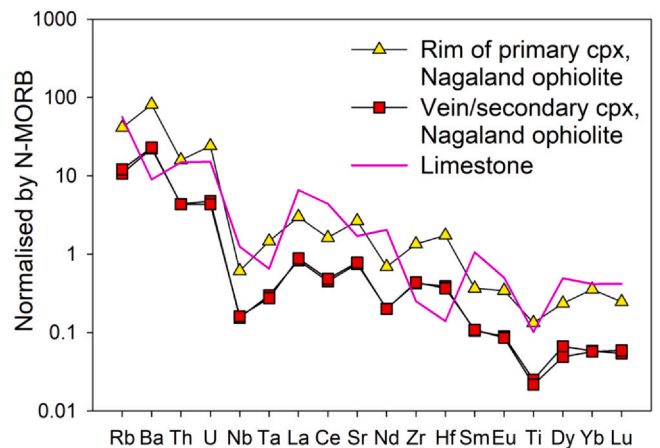
Fig. 11. N-MORB normalised trace elements patterns in secondary clinopyroxenes and rim of primary clinopyroxenes in the peridotites from the Nagaland ophiolites. Trace elements in limestone after Jin et al., (2009) are also plotted for comparison. We used trace elements data from Sun and McDonough, (1989) as normalising values.

elements into the overlying mantle, and that this process has affected the Nagaland and Manipur ophiolites investigated here.

6.5. Evolution of the Neo-Tethyan mantle

Different varieties of crustal mafic rocks and mantle peridotites with wide ranges of elemental and Nd isotopic abundances i.e., $\varepsilon_{Nd}(t)$ = −6.3 to +10.4 (Kingson et al., 2017, 2019) in the Nagaland and Manipur ophiolites indicate heterogeneous mantle source for these ophiolitic rocks. To decipher the events responsible for mantle source evolution and the origin of subsequent mantle heterogeneity in the Neo-Tethyan mantle preserved in the Nagaland and Manipur ophiolites, we contend that the depletion in Nb, Zr, Hf and Ti in N-MORB normalized trace element patterns could have resulted from mantle metasomatism as the first petrogenetic event during subduction. The LREE depletion observed in the studied primary clinopyroxenes (Fig. 4c and e) could then be produced by a larger extraction of melts from the carbonate metasomatised mantle as a second petrogenetic event. Such scenarios are supported by the compositional zoning of the studied clinopyroxenes (Fig. 12). However, zonation of certain elements and elemental ratios from core to rim in the clinopyroxenes (i.e., decrease in Na, Al and Zr/Hf towards rim, and an increase in Y, V, Ti and Ca/Al towards rim) present the following alternative possible explanations: (1) mobilization of selective elements during the serpentinization processes, (2) unequilibrated crystal growth from the same parental magma and (3) the interaction of melt with the residue (Shaw et al., 2006). The observed increase in fluid-immobile elements from core to rim (e.g., Y, Ti, V, etc.; Fig. 12) rules out the low-temperature serpentinization processes. In the case of unequilibrated crystal growth, the expected variation in Mg# [(Mg/(Mg+Fe^{+2})] is a decrease from core to rim, and not the increase in Mg# from core to rim as observed (Fig. 12), which rules out the crystal growth process as the cause of compositional zoning. Considering the data, and wider petrogenetic arguments, hypothesis 3 is more likely the cause of the elemental zoning based on the observed variations in Mg# and Ni/Zn since an increase in Mg# and Ni/Zn from core to rim (Fig. 12) indicates the interaction of the residual clinopyroxene with a new batch of mantle-derived melt.

A model of equilibrium partial melting of metasomatized mantle source in a subduction setting was used to test whether the clinopyroxene could be part of the residue. Assuming a carbonate-metasomatized mantle source, similar to the carbonate-metasomatized lherzolite sample 17JH24, after Guo et al., (2020), an equilibrium partial melting using the equation of Norman, (1998) was performed. The clinopyroxene in the lherzolite sample (17JH24) displays depletion in Nb, Ta,

O. Kingson, Y. Liu, R. Bhutani et al.
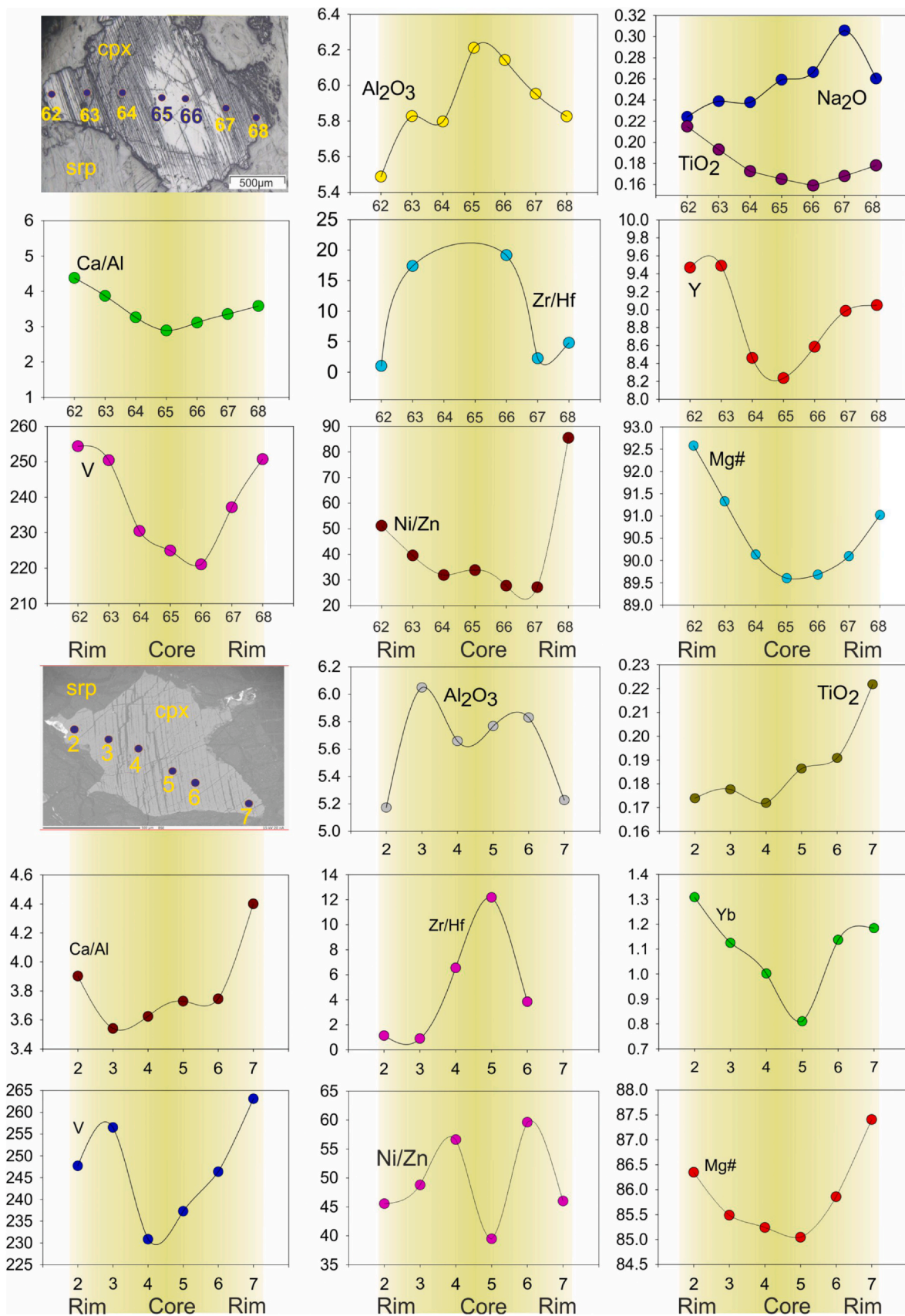
Fig. 12. Core to Rim elemental variations of selected clinopyroxene grains (primary) from the peridotite sample (MR14–5) in the Manipur ophiolite.
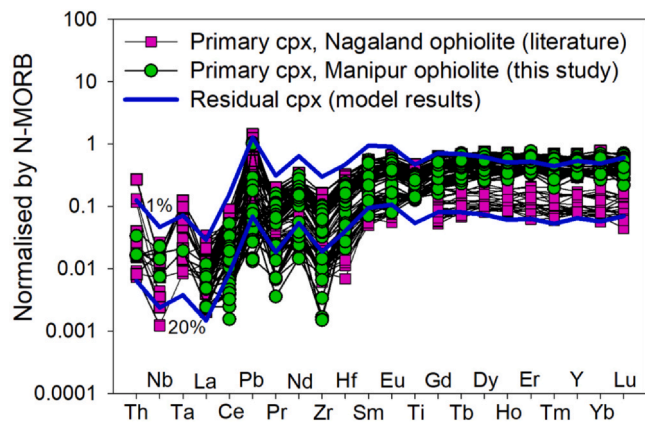
Fig. 13. N-MORB normalised trace elements patterns for resulting modelled residual clinopyroxenes compared with all the available and new trace elements patterns in clinopyroxenes of the peridotites from the Nagaland and Manipur ophiolites. Normalising values are from Sun and McDonough, (1989). Equilibrium partial melting equation after Normal (1998) was utilised for the geochemical model here. The carbonate-metasomatized lherzolite (sample no. 17JH24) after Guo et al. (2020) was assumed as a hypothetical mantle source for the model. The fraction of clinopyroxene in the source (X_{cpx}) was taken as 5% for the model. Partition coefficient for all the trace elements were taken from (Bedard, 2006; McKenzie and O'Nions, 1991; Frey, 1969; Irving and Frey, 1984).

Zr, Hf, Ti in N-MORB normalized spider diagram and enrichment in LREE compared to HREE in chondrite normalised patterns along with super-chondritic Zr/Hf (42.1–47.6), low Ti/Eu (1873–2115) and high $^{87}Sr/^{86}Sr$ (0.70527–0.70546) (Guo et al., 2020). Such geochemical and isotopic features are typical of a carbonate-metasomatized source (Guo et al., 2020; Zong and Liu, 2018; Chen et al., 2017, 2016; Wu et al., 2017). Therefore, the lherzolite sample (17JH24) was used as the carbonate-metasomatised source in this study since it has clinopyroxenes of similar geochemical signatures. [Note: Additional information about the parameters used in this model is given in the caption for Fig. 13]. The resulting model-generated residual solid (i.e., clinopyroxene) after 1–20% of equilibrium partial melting can explain the entire range of trace elements' abundances in clinopyroxenes of the Nagaland and Manipur ophiolites (Fig. 13). Using this model, we conclude that the peridotites in the Nagaland and Manipur ophiolites have been initially metasomatized and then have undergone equilibrium partial melting. These two petrogenetic events would then explain the mantle heterogeneity in the Neo-Tethyan mantle preserved in the Nagaland and Manipur ophiolites.

7. Petrogenetic and tectonic model explaining the origin for duality of geochemical signatures

A self-consistent model to explain the origin for duality of geochemical signatures found in the peridotites of the Nagaland and Manipur ophiolite belt is proposed (see also Fig. 14). During Neo-Tethyan oceanic-oceanic subduction at around 117 Ma (Fig. 14), a carbonate-rich fluid derived from the subducted limestone metasomatized the mantle wedge (Kingson et al., 2017, 2019). However, some portions of the same mantle wedge were less/not affected and remained unmetasomatized (Fig. 14). Accordingly, the peridotites samples with low ε_{Nd} (t) represent the metasomatized portions of the same mantle wedge, whilst the peridotite samples with higher ε_{Nd} (t) correspond to those unmetasomatized portions. At a later stage these two closely associated portions (i.e., metasomatized and un-metasomatized) of the same mantle wedge were obducted together and were emplaced to form the present-day exposure of subduction-related ophiolite mélange in the Indo-Burma Range, India.
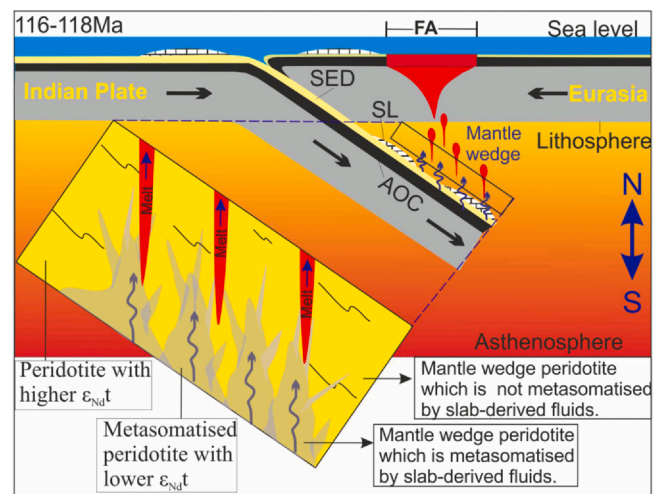
Fig. 14. A schematic diagram depicting origin of dual geochemical signatures (i.e., MOR- and SSZ-like geochemical affinity) in the peridotite of a same ophiolitic belt. Abbreviations: FA: fore-arc; SED: subducted sediment; SL: subducted limestone; AOC: altered basaltic oceanic crust.

8. Conclusions

Geochemical data from the whole-rock serpentinised peridotites and associated clinopyroxenes are presented, together with new in-situ major and trace element abundances from clinopyroxenes of the Nagaland and Manipur ophiolitic peridotites. From evaluation of these archive and new data, the following conclusions may be drawn:

1. The serpentinized peridotites in the Nagaland and Manipur ophiolites represent a relict of the Neo-Tethyan mantle wedge that underwent variable extents of mantle metasomatism and different degrees of partial melting.
2. Patchy metasomatism at the metre scale in the mantle wedge explains the apparent 'duality' of geochemical signatures observed in the ophiolite belt.
3. Carbonate-rich fluid derived from the subducted pelagic carbonate (limestone) represent one of the key metasomatic agents that fluxed the mantle wedge of the Neo-Tethyan mantle.
4. Two petrogenetic events (i.e., mantle metasomatism and partial melting) were responsible for the evolution and heterogeneity of the Neo-Tethyan mantle preserved in the Nagaland and Manipur ophiolites.

Data Availability

Data will be made available on request.

Declaration of Competing Interest

The authors declare that they have no known competing financial interests or personal relationships that could have appeared to influence the work reported in this paper.

Appendix A. Supporting information

Supplementary data associated with this article can be found in the online version at doi:10.1016/j.rines.2023.100001.

References

Abdullah, S., Misra, S., Ghosh, B., 2018. Melt-rock interaction and fractional crystallization in the Moho transition Zone: evidence from the cretaceous Naga Hills Ophiolite, North-East India. Lithos 322, 197–211. https://doi.org/10.1016/j.lithos.2018.10.012

Acharyya, S.K., Mitra, N.D., Nandy, D.R., 1986. Regional geology and tectonic setting of northeast India and adjoining region. Mem. Geol. Surv. India 119, 6–12.

Acharyya, S.K., 2010. Tectonic evolution of Indo-Burma range with special reference to Naga-Manipur Hills. Mem. Geol. Soc. India 75, 25–43.

Acharyya, S.K., 2015. Indo-Burma Range: a belt of accreted microcontinents, ophiolites and Mesozoic–Paleogeneflyschoid sediments. Int. J. Earth Sci 104, 1235–1251. https://doi.org/10.1007/s00531-015-1154-6

Acharyya, S.K., 2007. Collisional emplacement history of the Naga-Andaman ophiolites and the position of the eastern Indian suture. J. Asian Earth Sci 29, 229–242. https://doi.org/10.1016/j.jseaes.2006.03.003

Adam, J., Green, T., 2001. Experimentally determined partition coefficients for minor and trace elements in peridotite minerals and carbonatitic melt, and their relevance to natural carbonatites. Eur. J. Mineral. 13 (5), 815–827.

Aitchison, J.C., Ao, A., Bhowmik, S., Clarke, G.L., Ireland, T.R., Kachovich, S., Lokho, K., Stojanovic, D., Roeder, T., Truscott, N., Zhen, Y., Zhou, R., 2019. Tectonic evolution of the western margin of the burma microplate based on new fossil and radiometric age constraints. 2018TC005049. Tectonics. https://doi.org/10.1029/2018TC005049

Ahmed, A., Arai, S., 2002. Unexpectedly high-PGE chromitite from the deeper mantle section of the northern Oman ophiolite and its tectonic implications. Contr. Mineral. Petrol. 143 (3), 263–278.

Ahmed, A.H., Habtoor, A., 2015. Heterogeneously depleted Precambrian lithosphere deduced from mantle peridotites and associated chromitite deposits of Al'Ays ophiolite, Northwestern Arabian Shield, Saudi Arabia. Ore Geol. Rev. 67, 279–296.

Akizawa, N., Arai, S., Tamura, A., Uesugi, J., Python, M., 2011. Crustal diopsidites from the northern Oman ophiolite: Evidence for hydrothermal circulation through sub-oceanic Moho. J. Mineral. Petrol. Sci. 106 (5), 261–266.

Alabaster, T., Pearce, J.A., Malpas, J., 1982. The volcanic stratigraphy and petrogenesis of the Oman ophiolite complex. Contrib. Mineral. Petrol 81, 168–183. https://doi.org/10.1007/BF00371294

Anon, 1986. Geology of Nagaland ophiolite. Geol. Surv. India Memoir 119, 113.

Ao, A., Bhowmik, S.K., 2014. Cold subduction of the Neotethys: the metamorphic record from finely banded lawsonite and epidote-blueschists and associated metabasalts of the Nagaland Ophiolite Complex, India. J. Metamorph. Geol. 32, 829–860. https://doi.org/10.1111/jmg.12096

Ao, A., Bhowmik, S.K., Upadhyay, D., 2020. P-T-melt/fluid evolution of abyssal mantle peridotites from the Nagaland Ophiolite Complex, NE India: Geodynamic significance. Lithos 354–355. https://doi.org/10.1016/j.lithos.2019.105344

Ao, A., Satyanarayanan, M., 2022. Petrogenesis of mantle peridotite and cumulate peridotite rocks from the Nagaland Ophiolite Complex, NE India. Geological Journal 57 (2), 749–767.

Arai, S., 1997. Origin of podiform chromitites. J. Asian Earth Sci. 15 (2–3), 303–310.

Baker, M.B., Stolper, E.M., 1994. Determining the composition of high-pressure mantle melts using diamond aggregates. Geochim. Cosmochim. Acta 58, 2811–2827. https://doi.org/10.1016/0016-7037(94)90116-3

Batanova, V.G., Suhr, G., Sobolev, A.V., 1998. Origin of Geochemical Heterogeneity in the Mantle Peridotites from the Bay of Islands Ophiolite, Newfoundland, Canada: Ion Probe Study of Clinopyroxenes. Geochim. Cosmochim. Acta 62, 853–866. https://doi.org/10.1016/S0016-7037(97)00384-0

Baxter, A.T., Aitchison, J.C., Zyabrev, S.V., Ali, J.R., 2011. Upper Jurassic radiolarians from the Naga Ophiolite, Nagaland, northeast India. Gondwana Res. 20, 638–644. https://doi.org/10.1016/j.gr.2011.02.001

Bedard, J.H., 2006. A catalytic delamination-driven model for coupled genesis of Archaean crust and sub-continental lithospheric mantle. Geochim. Cosmochim. Acta 70, 1188–1214. https://doi.org/10.1016/j.gca.2005.11.008

Bhattacharjee, C.C., 1991. The ophiolites of northeast India — a subduction zone ophiolite complex of the Indo-Burmanorogenic belt. Tectonophysics 191, 213–222. https://doi.org/10.1016/0040-1951(91)90057-Y

Bhowmik, S.K., Ao, A., 2016. Subduction initiation in the Neo-Tethys: constraints from counterclockwise P-T paths in amphibolite rocks of the Nagaland Ophiolite Complex, India. J. Metamorph. Geol. 34, 17–44. https://doi.org/10.1111/jmg.12169

Bhowmik, S.K., Ao, A., Rajkakati, M., 2022. Tectonic framework of the high-pressure metamorphic rocks of the Nagaland Ophiolite Complex, North-east India, and its geodynamic significance: A review. Geological Journal 57 (2), 727–748.

Brey, G., Köhler, T., 1990. Geothermobarometry in four-phase lherzolites II. New thermobarometers, and practical assessment of existing thermobarometers. J. Petrol. 31, 1353–1378.

Brunschweiler, R.O., 1966. On the geology of the Indo–Burma ranges. J. Geol. Soc. Australia 13, 137–194.

Caciagli, N.C., Manning, C.E., 2003. The solubility of calcite in water at 6?16kbar and 500?800C. Contrib. Mineral. Petrol. 146, 275–285. https://doi.org/10.1007/s00410-003-0501-y

Caro, G., Bourdon, B., Birck, J.-L., Moorbath, S., 2006. High-precision 142Nd/144Nd measurements in terrestrial rocks: Constraints on the early differentiation of the Earth's mantle. Geochim. Cosmochim. Acta 70, 164–191. https://doi.org/10.1016/j.gca.2005.08.015

Chatterjee, N., Ghose, N.C., 2010. Metamorphic evolution of the Naga Hills eclogite and blueschist, Northeast India: implications for early subduction of the Indian plate under the Burma microplate. J. Metamorph. Geol 28, 209–225. https://doi.org/10.1111/j.1525-1314.2009.00861.x

Chen, C., Liu, Y., Foley, S.F., Ducea, M.N., Geng, X., Zhang, W., Xu, R., Hu, Z., Zhou, L., Wang, Z., 2017. Carbonated sediment recycling and its contribution to lithospheric refertilization under the northern North China Craton. Chem. Geol. 466, 641–653.

Coltorti, M., Bonadiman, C., Faccini, B., Ntaflos, T., Siena, F., 2007. Slab melt and intraplate metasomatism in Kapfenstein mantle xenoliths (Styrian Basin, Austria. Lithos 94, 66–89. https://doi.org/10.1016/j.lithos.2006.07.003

Coltorti, M., Bonadiman, C., Hinton, R.W., Siena, F., Upton, B.G.J., 1999. Carbonatite metasomatism of the oceanic upper mantle: evidence from clinopyroxenes and glasses in ultramafic xenoliths of grande comore, Indian Ocean. J. Petrol 40, 133–165. https://doi.org/10.1093/petroj/40.1.133

Curray, J.R., 2005. Tectonics and history of the Andaman Sea region. J. Asian Earth Sci 25, 187–232. https://doi.org/10.1016/j.jseaes.2004.09.001

Dalton, J.A., Wood, B.J., 1993. The compositions of primary carbonate melts and their evolution through wall rock reaction in the mantle. Earth Planet. Sci. Lett. 119, 511–525. https://doi.org/10.1016/0012-821X(93)90059-I

Deng, L., Liu, Y., Zong, K., Zhu, L., Xu, R., Hu, Z., Gao, S., 2017. Trace element and S r isotope records of multi-episode carbonatite metasomatism on the eastern margin of the North China Craton. Geochemistry, Geophysics, Geosyst. 18 (1), 220–237.

Dey, A., Hussain, M.F., Barman, M.N., 2018. Geochemical characteristics of mafic and ultramafic rocks from the Naga Hills Ophiolite, India: implications for petrogenesis. Geosci. Front. 9, 517–529. https://doi.org/10.1016/j.gsf.2017.05.006

Dilek, Y., Furnes, H., 2014. Ophiolites and their origins. Elements 10, 93–100. https://doi.org/10.2113/gselements.10.2.93

Dilek, Y., Furnes, H., 2009. Structure and geochemistry of Tethyan ophiolites and their petrogenesis in subduction rollback systems. Lithos 113 (1–2), 1–20.

Dilek, Y., Furnes, H., 2011. Ophiolite genesis and global tectonics: geochemical and tectonic fingerprinting of ancient oceanic lithosphere. Bulletin 123 (3–4), 387–411.

Dolejš, D., Manning, C.E., 2010. Thermodynamic model for mineral solubility in aqueous fluids: theory, calibration and application to model fluid-flow systems. Geofluids. https://doi.org/10.1111/j.1468-8123.2010.00282.x

Ellam, R.M., Hawkesworth, C.J., 1988. Elemental and isotopic variations in subduction related basalts: evidence for a three component model. Contrib. Mineral. Petrol. 98 (1), 72–80.

Ernewein, M., Pflumio, C., Whitechurch, H., 1988. The death of an accretion zone as evidenced by the magmatic history of the Sumail ophiolite (Oman). Tectonophysics 151 (1–4), 247–274.

Fareeduddin, Y.D., 2015. Structure and petrology of the Nagaland-Manipur Hill Ophiolitic Mélange zone, NE India: A Fossil Tethyan Subduction Channel at the India–Burma Plate Boundary. Episodes 38 (4), 298–314.

Falloon, T.J., Green, D.H., Danyushevsky, L.V., Faul, U.H., 1999. Peridotite melting at 1.0 and 1.5 GPa: an experimental evaluation of techniques using diamond aggregates and mineral mixes for determination of near-solidus melts. J. Petrol. 40, 1343–1375. https://doi.org/10.1093/petroj/40.9.1343

Fareeduddin, 2015. Structure and petrology of the nagaland-manipur hill ophiolite melange zone. Episodes. A Fossil TethyanSubduction Channel at the India - Burma Plate Boundary, NE India, pp. 38. https://doi.org/10.18814/epiiugs/2015/v38i4/82426

Frisby, C., Bizimis, M., Mallick, S., 2016. Hf–Nd isotope decoupling in bulk abyssal peridotites due to serpentinization. Chemical Geology 440, 60–72.

Frezzotti, M.L., Selverstone, J., Sharp, Z.D., Compagnoni, R., 2011. Carbonate dissolution during subduction revealed by diamond-bearing rocks from the Alps. Nat. Geosci. 4, 703–706. https://doi.org/10.1038/ngeo1246

Frey, F.A., 1969. Rare earth abundances in a high-temperature peridotite intrusion. Geochimica et Cosmochimica Acta 33 (11), 1429–1447.

Gass, I.G., 1968. Is the Troodos Massif of Cyprus a fragment of Mesozoic ocean floor? Nature 220 (5162), 39–42.

Gaetani, G.A., Grove, T.L., 1998. The influence of water on melting of mantle peridotite. Contrib. Mineral. Petrol. 131 (4), 323–346.

Gervasoni, F., Klemme, S., Rohrbach, A., Grützner, T., Berndt, J., 2017. Experimental constraints on mantle metasomatism caused by silicate and carbonate melts. Lithos 282–283, 173–186. https://doi.org/10.1016/j.lithos.2017.03.004

Ghose, N.C., Agrawal, O.P., Chatterjee, N., 2010. Geological and mineralogical study of eclogite and glaucophane schists in the Naga Hills Ophiolite, Northeast India: Naga Hills eclogite glaucophane schist. Isl. Arc 19, 336–356. https://doi.org/10.1111/j.1440-1738.2010.00710.x

Ghose, N.C., Chatterjee, N., Fareeduddin, 2014. A Petrographic Atlas of Ophiolite. Springer, India, New Delhi. https://doi.org/10.1007/978-81-322-1569-1

Ghosh, B., Bandyopadhyay, D., Morishita, T., 2017. Chapter 7 Andaman–Nicobar Ophiolites, India: origin, evolution and emplacement. Geol. Soc. Lond. Mem. 47, 95–110. https://doi.org/10.1144/M47.7

Ghosh, B., Mukhopadhyay, S., Morishita, T., Tamura, A., Arai, S., Bandyopadhyay, D., Chattopadhaya, S., Ovung, T.N., 2018. Diversity and evolution of suboceanic mantle: Constraints from Neotethyan ophiolites at the eastern margin of the Indian plate. J. Asian Earth Sci. 160, 67–77. https://doi.org/10.1016/j.jseaes.2018.04.010

Ghosh, B., Pal, T., Bhattacharya, A., Das, D., 2009. Petrogenetic implications of ophiolitic chromite from Rutland Island, Andaman—a boninitic parentage in supra-subduction setting. Mineral. Petrol. 96, 59–70. https://doi.org/10.1007/s00710-008-0039-9

Ghosh, B., Ray, J., Morishita, T., 2014. Grain-scale plastic deformation of chromite from podiformchromitite of the Naga-Manipur ophiolite belt. Ore Geol. Rev 56. Implication to mantle dynamics, India, pp. 199–208. https://doi.org/10.1016/j.oregeorev.2013.09.001

Green, D.H., Wallace, M.E., 1988. Mantle metasomatism by ephemeral carbonatite melts. Nature 336 (6198), 459–462.

Guice, G.L., McDonald, I., Hughes, H.S., Schlatter, D.M., Goodenough, K.M., MacDonald, J.M., Faithfull, J.W., 2018. Assessing the validity of negative high field strength-element anomalies as a proxy for Archaean subduction: evidence from the Ben Strome Complex. NW Scotland. Geosciences 8 (9), 338.

Guo, P., Ionov, D.A., Xu, W.L., Wang, C.G., Luan, J.P., 2020. Mantle and recycled oceanic crustal components in mantle xenoliths from northeastern China and their mantle sources. J. Geophys. Res. Solid Earth 125 (4).

Hu, Z., Gao, S., Liu, Y., Hu, S., Chen, H., Yuan, H., 2008. Signal enhancement in laser ablation ICP-MS by addition of nitrogen in the central channel gas. J. Anal. At. Spectrom 23, 1093. https://doi.org/10.1039/b804760j

Huang, J., Xiao, Y., Gao, Y., Hou, Z., Wu, W., 2012. Nb-Ta fractionation induced by fluid-rock interaction in subduction-zones: constraints from UHP eclogite- and vein-hosted rutile from the Dabieorogen. Central-Eastern China: J. Metamorph. Geol 30, 821–842. https://doi.org/10.1111/j.1525-1314.2012.01000.x

Ibotombi Singh, N., Debala Devi, L., Yaiphalembi Chanu, T., 2013. Petrological and geo-chemical study of serpentinised peridotites from the southern part of Manipur Ophiolitic Complex, Northeast India. Journal of the Geological Society of India 82 (2), 121–132.

Imchen, W., Thong, G.T., Pongen, T., 2014. Provenance, tectonic setting and age of the sediments of the Upper Disang Formation in the Phek District, Nagaland. J. Asian Earth Sci. 88, 11–27. https://doi.org/10.1016/j.jseaes.2014.02.027

Ionov, D.A., Dupuy, C., O'Reilly, S.Y., Kopylova, M.G., Genshaft, Y.S., 1993. Carbonated peridotite xenoliths from Spitsbergen: implications for trace element signature of mantle carbonate metasomatism. Earth Planet. Sci. Lett. 119, 283–297. https://doi.org/10.1016/0012-821X(93)90139-Z

Irving, A.J., Frey, F.A., 1984. Trace element abundances in megacrysts and their host basalts: constraints on partition coefficients and megacryst genesis. Geochimica et Cosmochimica Acta 48 (6), 1201–1221.

Ishizuka, O., Tani, K., Reagan, M.K., 2014. Izu-Bonin-Mariana forearc crust as a modern ophiolite analogue. Elements 10 (2), 115–120.

Ishizuka, O., Tani, K., Reagan, M.K., Kanayama, K., Umino, S., Harigane, Y., Sakamoto, I., Miyajima, Y., Yuasa, M., Dunkley, D.J., 2011. The timescales of subduction initiation and subsequent evolution of an oceanic island arc. Earth Planet. Sci. Lett. 306, 229–240. https://doi.org/10.1016/j.epsl.2011.04.006

Jana, S.K., Acharyya, S.K., 1986. Geological map around Phokphur, Tuensang district, Nagaland (Type Section Phokphur Formation). In: Anonymous (Ed.), Geology of Nagaland ophiolite D.B. Ghosh Commemorative Volume, Geological Survey of India Memoir 119 Calcutta: Plate III, Geological Survey of India.

Jin, Z., Zhu, D., Hu, W., Zhang, X., Zhang, J., Song, Y., 2009. Mesogenetic dissolution of the middle Ordovician limestone in the Tahe oilfield of Tarim basin, NW China. Marine Petrol. Geol. 26 (6), 753–763.

Jones, A.P., Genge, M., Carmody, L., 2013. Carbonate melts and carbonatites. Rev. Mineral. Geochem. 75, 289–322. https://doi.org/10.2138/rmg.2013.75.10

Khedr, M.Z., Arai, S., Python, M., Tamura, A., 2014. Chemical variations of abyssal peridotites in the central Oman ophiolite: Evidence of oceanic mantle heterogeneity. Gondwana Res. 25, 1242–1262. https://doi.org/10.1016/j.gr.2013.05.010

Kingson, O., Bhutani, R., Balakrishnan, S., Dash, J.K., Shukla, A.D., 2019. Subduction-related Manipur Ophiolite Complex, Indo-Myanmar Ranges: elemental and isotopic record of mantle metasomatism. Geol. Soc. Lond. Spec. Publ. SP481.9. https://doi.org/10.1144/SP481.9

Kingson, O., Bhutani, R., Dash, J.K., Sebastian, S., Balakrishnan, S., 2017. Resolving the conundrum in origin of the Manipur Ophiolite Complex, Indo-Myanmar range: constraints from Nd isotopic ratios and elemental concentrations in serpentinized peridotite. Chem. Geol. 460, 117–129. https://doi.org/10.1016/j.chemgeo.2017.04.021

Klemme, S., van der Laan, S.R., Foley, S.F., Günther, D., 1995. Experimentally determined trace and minor element partitioning between clinopyroxene and carbonate melt under upper mantle conditions. Earth Planet. Sci. Lett. 133, 439–448. https://doi.org/10.1016/0012-821X(95)00098-W

Li, Yuan-Hui, 1991. Distribution patterns of the elements in the ocean: A synthesis. Geochimica et Cosmochimica Acta 55 (11), 3223–3240.

Li, J.-L., Gao, J., John, T., Klemd, R., Su, W., 2013. Fluid mediated metal transport in subduction zones and its link to arc-related giant ore deposits: constraints from a sulfide-bearing HP vein in lawsonite-eclogite (Tianshan, China). Geochim. Cosmochim. Acta 120, 326–362.

Li, J.-L., John, T., Gao, J., Klemd, R., Wang, X.-S., 2017. Subduction channel fluid–rock interaction and mass transfer: Constraints from a retrograde vein in blueschist (SW Tianshan, China). Chem. Geol. 456, 28–42.

Li, H.Y., Chen, R.-X., Zheng, Y.-F., Hu, Z., Xu, L., 2018. Crustal metasomatism at the slab-mantle interface in a continental subduction channel: geochemical evidence from orogenic peridotite in the sulu orogen. J. Geophys. Res. Solid Earth 123, 2174–2198. https://doi.org/10.1002/2017JB014015

Liu, C.-Z., Chung, S.-L., Wu, F.-Y., Zhang, C., Xu, Y., Wang, J.-G., Chen, Y., Guo, S., 2016a. Tethyan suturing in Southeast Asia: Zircon U-Pb and Hf-O isotopic constraints from Myanmar ophiolites. Geology 44, 311–314. https://doi.org/10.1130/G37342.1

Liu, C.-Z., Zhang, C., Xu, Y., Wang, J.-G., Chen, Y., Guo, S., Wu, F.-Y., Sein, K., 2016b. Petrology and geochemistry of mantle peridotites from the Kalaymyo and Myitkyina ophiolites (Myanmar): Implications for tectonic settings. Lithos 264, 495–508. https://doi.org/10.1016/j.lithos.2016.09.013

Liu, Y., Gao, S., Kelemen, P.B., Xu, W., 2008. Recycled crust controls contrasting source compositions of Mesozoic and Cenozoic basalts in the North China Craton. Geochim. Cosmochim. Acta 72, 2349–2376. https://doi.org/10.1016/j.gca.2008.02.018

Maibam, B., Foley, S., Luguet, A., Jacob, D.E., Singh, T.B., Ray, D., Panda, D.K., Keppler, R., 2017. Characterisation of chromites, chromite hosted inclusions of silicates and metal alloys in chromitites from the Indo-Myanmar ophiolite belt of Northeastern India. Ore Geol. Rev. 90, 260–273. https://doi.org/10.1016/j.oregeorev.2017.05.032

Marchesi, C., Garrido, C.J., Proenza, J.A., Hidas, K., Varas-Reus, M.I., Butjosa, L., Lewis, J.F., 2016. Geochemical record of subduction initiation in the sub-arc mantle: in-sights from the Loma Caribe peridotite (Dominican Republic). Lithos 252, 1–15.

McKenzie, D., O'Nions, R.K., 1991. Partial melt distributions from inversion of rare earth element concentrations. J. Petrol. 32, 1021–1091. https://doi.org/10.1093/petrology/32.5.1021

Meinhold, G., 2010. Rutile and its applications in earth sciences. Earth-Sci. Rev. 102, 1–28. https://doi.org/10.1016/j.earscirev.2010.06.001

Metcalf, R.V., Shervais, J.W., 2008. Supra subduction-zone ophiolites: Is there really an ophiolite conundrum? Spec. Papers-Geol. Soc. Am. 438, 191.

Miyashiro, A., 1973. The Troodos ophiolitic complex was probably formed in an island arc. Earth Planet. Sci. Lett. 19, 218–224. https://doi.org/10.1016/0012-821X(73)90118-0

Moyen, J.-F., 2009. High Sr/Y and La/Yb ratios: The meaning of the "adakitic signature. Lithos 112, 556–574. https://doi.org/10.1016/j.lithos.2009.04.001

Moores, E.M., Vine, F.J., 1971. The Troodos Massif, Cyprus and other ophiolites as oceanic crust: evaluation and implications. Philosophical Transactions of the Royal Society of London. Series A, Mathematical and Physical Sciences 268 (1192), 443–467.

Munker, C., Wörner, G., Yogodzinski, G., Churikova, T., 2004. Behaviour of high field strength elements in subduction zones: constraints from Kamchatka–Aleutian arc lavas. Earth Planet. Sci. Lett. 224, 275–293. https://doi.org/10.1016/j.epsl.2004.05.030

Ningthoujam, P.S., Dubey, C.S., Guillot, S., Fagion, A.S., Shukla, D.P., 2012. Origin and serpentinization of ultramafic rocks of Manipur Ophiolite Complex in the Indo-Myanmar subduction zone, Northeast India. Journal of Asian Earth Sciences 50, 128–140.

Norman, M.D., 1998. Melting and metasomatism in the continental lithosphere: laser ablation ICPMS analysis of minerals in spinel lherzolites from eastern Australia. Contrib. Mineral. Petrol. 130 (3–4), 240–255.

O'Driscoll, B., Day, J.M.D., Walker, R.J., Daly, J.S., McDonough, W.F., Piccoli, P.M., 2012. Chemical heterogeneity in the upper mantle recorded by peridotites and chromitites from the Shetland Ophiolite Complex, Scotland. Earth Planet. Sci. Lett. 333–334, 226–237. https://doi.org/10.1016/j.epsl.2012.03.035

O'Driscoll, B., Walker, R.J., Clay, P.L., Day, J.M.D., Ash, R.D., Daly, J.S., 2018. Length-scales of chemical and isotopic heterogeneity in the mantle section of the Shetland Ophiolite Complex, Scotland. Earth Planet. Sci. Lett. 488, 144–154. https://doi.org/10.1016/j.epsl.2018.02.020

O'Reilly, S.Y., Griffin, W.L., 2013. Mantle Metasomatism, in: Metasomatism and the Chemical Transformation of Rock. Lecture Notes in Earth System Sciences. Springer Berlin Heidelberg, Berlin, Heidelberg, pp. 471–533. https://doi.org/10.1007/978-3-642-28394-9_12

Ovung, T.N., Ray, J., Ghosh, B., Koeberl, C., Topa, D., Paul, M., 2018. Clinopyroxene composition of volcanics from the Manipur Ophiolite, Northeastern India: implica-tions to geodynamic setting. Int. J. Earth Sci 107, 1215–1229. https://doi.org/10.1007/s00531-017-1529-y

Ovung, T.N., Ghosh, B., Ray, J., 2020. Petrogenesis of neo-Tethyan ophiolites from the Indo-Myanmar ranges: a review. Int. Geol. Rev. 1–13. https://doi.org/10.1080/00206814.2020.1775137

Ovung, T.N., Ray, J., Teng, X., Ghosh, B., Paul, M., Ganguly, P., Sengupta, S., Das, S., 2017. Mineralogy of the Manipur Ophiolite Belt, North East India: implications for mid-oceanic ridge and supra-subduction zone origin. Current Science 2122–2129.

Palme, H., O'Neill, H.S.C., Holland, H.D. and Turekian, K.K., 2014. Treatise on geo-chemistry. 2nd ed, p.15.

Pal, T., Bhattacharya, A., Nagendran, G., Yanthan, N.M., Singh, R., Raghumani, N., 2014. Petrogenesis of chromites from the Manipur ophiolite belt, NE India: evidence for a supra-subduction zone setting prior to Indo-Myanmar collision. Mineral. Petrol. 108, 713–726. https://doi.org/10.1007/s00710-014-0320-z

Pandey, R., Rao, N.C., Pandit, D., Sahoo, S., Dhote, P., 2018. Imprints of modal meta-somatism in the post-Deccan subcontinental lithospheric mantle: petrological evi-dence from an ultramafic xenolith in an Eocene lamprophyre, NW India. Geological Society, London, Special Publications, 463(1), pp.117–136.

Peacock, S.M., 2013. Thermal and Petrologic Structure of Subduction Zones. In: Bebout, G.E., Scholl, D.W., Kirby, S.H., Platt, J.P. (Eds.), Geophysical Monograph Series. American Geophysical Union, Washington, D. C, pp. 119–133. https://doi.org/10.1029/GM096p0119

Peacock, S.M., 1991. Numerical simulation of subduction zone pressure-temperature-time paths: constraints on fluid production and arc magmatism. Philos. Trans. R. Soc. Lond. Ser. Phys. Eng. Sci. 335, 341–353. https://doi.org/10.1098/rsta.1991.0050

Pearce, J.A., 2008. Geochemical fingerprinting of oceanic basalts with applications to ophiolite classification and the search for Archean oceanic crust. Lithos 100 (1–4), 14–48.

Pearce, J.A., Lippard, S.J., Roberts, S., 1984. Characteristics and tectonic significance of supra-subduction zone ophiolites. Geol. Soc. Lond. Spec. Publ. 16, 77–94. https://doi.org/10.1144/GSL.SP.1984.016.01.06

Pearce, J.A., Robinson, P.T., 2010. The Troodos ophiolitic complex probably formed in a subduction initiation, slab edge setting. Gondwana Res. 18, 60–81.

Peters, D., Bretscher, A., John, T., Scambelluri, M., Pettke, T., 2017. Fluid-mobile elements in serpentinites: constraints on serpentinisation environments and element cycling in subduction zones. Chem. Geol. 466, 654–666.

Petrological database of the ocean floor, information system for geochemical data of igneous and metamorphic rocks from the ocean floor, 2001 URL http://www.petdb.org/.

Pfänder, J.A., Münker, C., Stracke, A., Mezger, K., 2007. Nb/Ta and Zr/Hf in ocean island basalts — implications for crust–mantle differentiation and the fate of Niobium. Earth Planet. Sci. Lett. 254, 158–172. https://doi.org/10.1016/j.epsl.2006.11.027

Pickering-Witter, J., Johnston, A.D., 2000. The effects of variable bulk composition on the melting systematics of fertile peridotitic assemblages. Contrib. Mineral. Petrol. 140 (2), 190–211.

Pirard, C., Hermann, J., O'Neill, H.S.C., 2013. Petrology and geochemistry of the crust–mantle boundary in a nascent arc, Massif du Sud ophiolite, New Caledonia, SW Pacific. Journal of Petrology 54 (9), 1759–1792.

Plank, T., Langmuir, C.H., 1998. The chemical composition of subducting sediment and its consequences for the crust and mantle. Chem. Geol. 145 (3–4), 325–394.

Plank, T., 2014. The chemical composition of subducting sediments. Elsevier.

Poli, S., 2015. Carbon mobilized at shallow depths in subduction zones by carbonatitic liquids. Nat. Geosci. 8, 633–636. https://doi.org/10.1038/ngeo2464

Poli, S., Franzolin, E., Fumagalli, P., Crottini, A., 2009. The transport of carbon and hydrogen in subducted oceanic crust: an experimental study to 5 GPa. Earth Planet. Sci. Lett. 278, 350–360. https://doi.org/10.1016/j.epsl.2008.12.022

Python, M., Ceuleneer, G., Ishida, Y., Barrat, J.A., Arai, S., 2007. Oman diopsidites: a new lithology diagnostic of very high temperature hydrothermal circulation in mantle peridotite below oceanic spreading centres. Earth Planetary Sci. Lett. 255 (3–4), 289–305.

Python, M., Ceuleneer, G., 2003. Nature and distribution of dykes and related melt migration structures in the mantle section of the Oman ophiolite. Geochem. Geophys. Geosyst. 4, 7.

Rajkakati, M., Bhowmik, S.K., Ao, A., Ireland, T.R., Avila, J., Clarke, G.L., Bhandari, A., Aitchison, J.C., 2019. Thermal history of Early Jurassic eclogite facies metamorphism in the Nagaland Ophiolite Complex, NE India: New insights into pre-Cretaceous subduction channel tectonics within the. Neo-Tethys. Lithos 346, 105166.

Reagan, M.K., Ishizuka, O., Stern, R.J., Kelley, K., Ohara, Y., Blichert-Toft, J., Bloomer, S.H., Cash, J., Fryer, P., Hanan, B.B., Hickey-Vargas, R., Ishii, T., Kimura, J.-I., Peate, D.W., Rowe, M.C., Woods, M., 2010. Fore-arc basalts and subduction initiation in the Izu-Bonin-Mariana system: Geochem. Geophys (n/a-n/a). Geosystems 11. https://doi.org/10.1029/2009GC002871

Rivalenti, G., Vannucci, R., Rampone, E., Mazzucchelli, M., Piccardo, G.B., Piccirillo, E.M., Bottazzi, P., Ottolini, L., 1996. Peridotite clinopyroxene chemistry reflects mantle processes rather than continental versus oceanic settings. Earth Planet. Sci. Lett. 139, 423–437. https://doi.org/10.1016/0012-821X(96)00019-2

Roden, M.F., Murthy, V.R., 1985. Mantle metasomatism. Annu. Rev. Earth Planet. Sci. 13, 269–296. https://doi.org/10.1146/annurev.ea.13.050185.001413

Rollinson, H., Gravestock, P., 2012. The trace element geochemistry of clinopyroxenes from pyroxenites in the Lewisian of NW Scotland: insights into light rare earth element mobility during granulite facies metamorphism. Contrib. Mineral. Petrol. 163 (2), 319–335.

Rudnick, R.L., McDonough, W.F., Chappellz, B.W., 1993. Carbonatite metasomatism in the northern Tanzanian mantle: Petrographic and geochemical characteristics. Earth Planet. Sci. Lett. 114, 463–475. https://doi.org/10.1016/0012-821X(93)90076-L

Ryan, W.B.F., Carbotte, S.M., Coplan, J.O., O'Hara, S., Melkonian, A., Arko, R., Weissel, R.A., Ferrini, V., Goodwillie, A., Nitsche, F., Bonczkowski, J., Zemsky, R., 2009. Global Multi-Resolution Topography synthesis (n/a-n/a). Geochem. Geophys. Geosyst. 10. https://doi.org/10.1029/2008GC002332

Salters, V.J., Stracke, A., 2004. Composition of the depleted mantle. Geochemistry, Geophysics, Geosystems 5 (5).

Saccani, E., 2015. A new method of discriminating different types of post-Archean ophiolitic basalts and their tectonic significance using Th-Nb and Ce-Dy-Yb systematics. Geosci. Front. 6 (4), 481–501.

Schwab, B.E., Johnston, A.D., 2001. Melting systematics of modally variable, compositionally intermediate peridotites and the effects of mineral fertility. J. Petrol 42, 1789–1811. https://doi.org/10.1093/petrology/42.10.1789

Sengupta, S., Acharyya, S.K., Van Den Hul, H.J., Chattopadhyay, B., 1989. Geochemistry of volcanic rocks from the Naga Hills Ophiolites, northeast India and their inferred tectonic setting. J. Geol. Soc. 146, 491–498. https://doi.org/10.1144/gsjgs.146.3.0491

Sengupta, S., Ray, K.K., Acharyya, S.K., de Smeth, J.B., 1990. Nature of ophiolite occurrences along the eastern margin of the Indian plate and their tectonic significance. Geology 18, 439. https://doi.org/10.1130/0091-7613(1990)018<0439:NOOOAT>2.3.CO;2

Shaw, C.S.J., Heidelbach, F., Dingwell, D.B., 2006. The origin of reaction textures in mantle peridotite xenoliths from Sal Island. Contrib. Mineral. Petrol 151. the case for "metasomatism" by the host lava, Cape Verde, pp. 681–697. https://doi.org/10.1007/s00410-006-0087-2

Sharma, M., Wasserburg, G.J., 1996. The neodymium isotopic compositions and rare earth patterns in highly depleted ultramafic rocks. Geochim. Cosmochim. Acta 60 (22), 4537–4550.

Singh, A.K., 2013. Petrology and geochemistry of Abyssal Peridotites from the Manipur Ophiolite Complex, Indo-Myanmar Orogenic Belt, Northeast India: implication for

melt generation in mid-oceanic ridge environment. J. Asian Earth Sci. 66, 258–276. https://doi.org/10.1016/j.jseaes.2013.02.004

Singh, A.K., Chung, S.-L., Bikramaditya, R.K., Lee, H.Y., 2017. New U–Pb zircon ages of plagiogranites from the Nagaland–Manipur Ophiolites, Indo-Myanmar Orogenic Belt, NE India. J. Geol. Soc. 174, 170–179. https://doi.org/10.1144/jgs2016-048

Singh, A.K., Khogenkumar, S., Singh, L.R., Bikramaditya, R.K., Khuman, Ch.M., Thakur, S.S., 2016. Evidence of Mid-ocean ridge and shallow subduction forearc magmatism in the Nagaland-Manipur ophiolites, northeast India: constraints from mineralogy and geochemistry of gabbros and associated mafic dykes. Chem. Erde - Geochem. 76, 605–620. https://doi.org/10.1016/j.chemer.2016.09.002

Singh, A.K., Tewari, V.C., Sial, A.N., Khanna, P.P., Singh, N.I., 2016. Rare earth elements and stable isotope geochemistry of carbonates from the mélange zone of Manipur ophiolitic Complex, Indo-Myanmar Orogenic Belt, Northeast India. Carbonates and evaporites 31, 139–151.

Sloan, R.A., Elliott, J.R., Searle, M.P., Morley, C.K., 2017. Active tectonics of Myanmar and the Andaman Sea. Geol. Soc. Lond. Mem. 48, 19–52. https://doi.org/10.1144/M48.2

Soibam, I., Khuman, M.Ch, Subhamenon, S.S., 2015. Ophiolitic rocks of the Indo-Myanmar Ranges, NE India: relicts of an inverted and tectonically imbricated hyper-extended continental margin basin? Geol. Soc. Lond. Spec. Publ 413, 301–331. https://doi.org/10.1144/SP413.12

Spandler, C., Pirard, C., 2013. Element recycling from subducting slabs to arc crust: a review. Lithos 170–171, 208–223. https://doi.org/10.1016/j.lithos.2013.02.016

Stern, R.J., 2004. Subduction initiation: spontaneous and induced. Earth Planet. Sci. Lett. 226, 275–292. https://doi.org/10.1016/j.epsl.2004.08.007

Stracke, A., 2012. Earth's heterogeneous mantle: a product of convection-driven interaction between crust and mantle. Chem. Geol. 330–331, 274–299. https://doi.org/10.1016/j.chemgeo.2012.08.007

Sun, J., Liu, C.-Z., Wu, F.-Y., Yang, Y.-H., Chu, Z.-Y., 2012. Metasomatic origin of clinopyroxene in Archean mantle xenoliths from Hebi, North China Craton: trace-element and Sr-isotope constraints. Chem. Geol. 328, 123–136. https://doi.org/10.1016/j.chemgeo.2012.03.014

Sun, S., McDonough, W.F., 1989. Chemical and isotopic systematics of oceanic basalts: implications for mantle composition and processes. Geol. Soc. Lond. Spec. Publ. 42, 313–345. https://doi.org/10.1144/GSL.SP.1989.042.01.19

Taylor, W.R., 1998. An experimental test of some geothermometer and geobarometer formulations for upper mantle peridotites with application to the thermobarometry of fertile lherzolite and garnet websterite. Neues Jahrbuch Mineralogie-Abhandlungen 172, 381–408.

Uysal, I., Tarkian, M., Sadiklar, M.B., Zaccarini, F., Meisel, T., Garuti, G., Heidrich, S., 2009. Petrology of Al-and Cr-rich ophiolitic chromitites from the Muğla, SW Turkey: implications from composition of chromite, solid inclusions of platinum-group mineral, silicate, and base-metal mineral, and Os-isotope geochemistry. Contrib. Mineral. Petrol. 158 (5), 659–674.

Uysal, I., Akmaz, R.M., Kapsiotis, A., Demir, Y., Saka, S., Avcı, E., Mueller, D., 2015. Genesis and geodynamic significance of chromitites from the Orhaneli and Harmancık ophiolites (Bursa, NW Turkey) as evidenced by mineralogical and compositional data. Ore Geol. Rev. 65, 26–41.

Uysal, I., Ersoy, E.Y., Dilek, Y., Kapsiotis, A., Sarıfakıoğlu, E., 2016. Multiple episodes of partial melting, depletion, metasomatism and enrichment processes recorded in the heterogeneous upper mantle sequence of the Neotethyan Eldivan ophiolite, Turkey. Lithos 246, 228–245.

Uysal, I., Kapsiotis, A., Akmaz, R.M., Saka, S., Seitz, H.M., 2018. The Guleman ophiolitic chromitites (SE Turkey) and their link to a compositionally evolving mantle source during subduction initiation. Ore Geol. Rev. 93, 98–113.

Vadlamani, R., Wu, F.-Y., Ji, W.-Q., 2015. Detrital zircon U–Pb age and Hf isotopic composition from foreland sediments of the Assam Basin, NE India: constraints on sediment provenance and tectonics of the Eastern Himalaya. J. Asian Earth Sci. 111, 254–267. https://doi.org/10.1016/j.jseaes.2015.07.011

Verencar, A., Saha, A., Ganguly, S., Manikyamba, C., 2021. Tectono-magmatic evolution of Tethyan oceanic lithosphere in supra subduction zone fore arc regime: Geochemical fingerprints from crust-mantle sections of Naga Hills Ophiolite. Geoscience Frontiers 12 (3), 101096.

Verencar, A., Saha, A., Ganguly, S., Satyanarayanan, M., Doley, B., Mohan, M.R., 2022. Multistage melt impregnation in Tethyan oceanic mantle: Petrochemical constraints from channelized melt flow in the Naga Hills Ophiolite. Geochemistry 82 (1), 125821.

Vidyadharan, K.T., Srivastava, R.K., Bhattacharyya, S., Joshi, A., Jena, S.K., 1986. Distribution and description of major rock types. Memoirs of the Geological Survey of India 119, 18–27.

Walter, M.J., 1998. Melting of garnet peridotite and the origin of komatiite and depleted lithosphere. J. Petrol 39, 29–60. https://doi.org/10.1093/petroj/39.1.29

Wang, C., Jin, Z., Gao, S., Zhang, J., Zheng, S., 2010. Eclogite-melt/peridotite reaction: experimental constrains on the destruction mechanism of the North China Craton. Sci. China Earth Sci. 53, 797–809. https://doi.org/10.1007/s11430-010-3084-2

Wasylenki, L.E., 2003. Near-solidus melting of the shallow upper mantle: partial melting experiments on depleted peridotite. J. Petrol 44, 1163–1191. https://doi.org/10.1093/petrology/44.7.1163

Whattam, S.A., Stern, R.J., 2011. The 'subduction initiation rule': a key for linking ophiolites, intra-oceanic forearcs, and subduction initiation. Contrib. Mineral. Petrol. 162, 1031–1045. https://doi.org/10.1007/s00410-011-0638-z

Workman, R.K., Hart, S.R., 2005. Major and trace element composition of the depleted MORB mantle (DMM). Earth Planetary Sci. Lett. 231 (1–2), 53–72.

Wu, D., Liu, Y., Chen, C., Xu, R., Ducea, M.N., Hu, Z., Zong, K., 2017. In-situ trace element and Sr isotopic compositions of mantle xenoliths constrain two-stage metasomatism beneath the northern North China Craton. Lithos 288, 338–351.

Wu, W., Yang, J., Dilek, Y., Milushi, I., Lian, D., 2018. Multiple episodes of melting, depletion, and enrichment of the Tethyan mantle: petrogenesis of the peridotites and chromitites in the Jurassic Skenderbeu massif, Mirdita ophiolite, Albania. Lithosphere 10 (1), 54–78.

Xu, C., Campbell, I.H., Kynicky, J., Allen, C.M., Chen, Y., Huang, Z., Qi, L., 2008. Comparison of the Daluxiang and Maoniuping carbonatitic REE deposits with Bayan Obo REE deposit, China. Lithos 106 (1-2), 12–24.

Yaxley, G.M., Crawford, A.J., Green, D.H., 1991. Evidence for carbonatite metasomatism in spinel peridotite xenoliths from western Victoria, Australia. Earth Planet. Sci. Lett. 107, 305–317. https://doi.org/10.1016/0012-821X(91)90078-V

Zhang, P.F., Zhou, M.F., Yumul Jr, G.P., 2020. Coexistence of high-Al and high-Cr chromite orebodies in the Acoje block of the Zambales ophiolite. Ore Geology Reviews 126 Evidence for subduction initiation, Philippines, 103739.

Zheng, Y.-F., 2012. Metamorphic chemical geodynamics in continental subduction zones. Chem. Geol. 328, 5–48. https://doi.org/10.1016/j.chemgeo.2012.02.005

Zheng, Y.-F., Hermann, J., 2014. Geochemistry of continental subduction-zone fluids. Earth Planets Space 66, 93. https://doi.org/10.1186/1880-5981-66-93

Zhou, M.F., Robinson, P.T., Malpas, J., Li, Z., 1996. Podiform chromitites in the Luobusa ophiolite (southern Tibet): implications for melt-rock interaction and chromite segregation in the upper mantle. J. Petrol. 37 (1), 3–21.

Zhou, M.F., Sun, M., Keays, R.R., Kerrich, R.W., 1998. Controls on platinum-group elemental distributions of podiform chromitites: a case study of high-Cr and high-Al chromitites from Chinese orogenic belts. Geochim. Cosmochim. Acta 62 (4), 677–688.

Zong, K., Liu, Y., 2018. Carbonate metasomatism in the lithospheric mantle: implications for cratonic destruction in North China. Sci. China Earth Sci. 61, 711–729. https://doi.org/10.1007/s11430-017-9185-2